Economic Geology, v. 118, no. 6, pp. 1261–1290

Geology of Porphyry Cu-Au and Epithermal Cu-Au-Ag Mineralization at Filo del Sol, Argentina-Chile: Extreme Telescoping During Andean Uplift

José Perelló,[1,†] Richard H. Sillitoe,[2] Joaquín Rossello,[3,*] Julián Forestier,[3] Guido Merino,[3] and Diego Charchaflié[3]

[1]*Blaise Cendrars 6736, Vitacura, Santiago, Chile*

[2]*27 West Hill Park, Highgate Village, London N6 6ND, England*

[3]*Filo Mining Corporation, Gorriti 4855, CABA, Buenos Aires, Argentina*

Abstract

Filo del Sol is a composite porphyry-epithermal deposit, straddling the frontier between Argentina and Chile at latitude 28°29′ S, that has attracted a great deal of recent attention because of several drill intersections in excess of 1 km long with unusually high Cu, Au, and Ag grades. The deposit is part of the 8.5-km-long, N- to NE-trending Filo del Sol alignment of porphyry and high-sulfidation epithermal centers, which, in turn, is located in the newly defined Vicuña metallogenic belt that unites the well-known late Oligocene to middle Miocene Maricunga and El Indio belts. The deposit is hosted by Permian felsic volcanic rocks intruded by Triassic monzogranite and, nearer the surface, by shallowly dipping Late Cretaceous volcano-sedimentary rocks. These lithologic units were intruded by several generations of mafic dikes and high-level sills and, in the middle Miocene, by a parallel swarm of composite diorite porphyry dikes. An intermineral magmatic-hydrothermal breccia body is closely associated with the porphyry dikes and subsequently cut at shallow levels by a smaller, finer-grained breccia of phreatic and, possibly, phreatomagmatic origin. Early Cu-Au mineralization, mainly as chalcopyrite, is associated with K-feldspar- and biotite-bearing potassic alteration and accompanying A-type quartz-veinlet stockworks. The potassic zone was massively overprinted and extensively reconstituted by a zone of vuggy residual quartz and silicification in the core of the deposit, flanked by quartz-alunite as part of a more extensive lithocap. These alteration types host high-sulfidation Cu-Au-Ag mineralization as pyrite with early enargite and later bornite, chalcocite, covellite, and numerous Ag-bearing sulfosalts, with the highest grades typically confined to vuggy residual quartz. Largely barren, steam-heated alteration is preserved above and overprinted on the lithocap. The results of radiometric dating (six U-Pb and 22 Re-Os ages) show that porphyry intrusion and potassic alteration began at ~15 Ma and lasted for nearly 1 m.y., although most of the molybdenite samples reported ages from 14.7 to 14.4 ± 0.06 Ma. This short interval coincided with a pulse of regional compressive tectonism accommodated by high-angle, thick-skinned, reverse faulting of basement-cored blocks, and concomitant uplift and exhumation. This uplift gave rise to ~1 km of erosion during formation of the Filo del Sol deposit, thereby accounting for the extreme telescoping of high-sulfidation over porphyry mineralization. Spatial association of these middle Miocene intrusion centers with dated middle Permian and Eocene mineralization suggests deep-seated structural control of the Filo del Sol alignment. Ongoing supergene processes under low-pH conditions produced a near-surface resource dominated by chalcanthite, with minor underlying chalcocite enrichment, as well as partially oxidizing a shallow zone of high-grade Ag mineralization.

Introduction

The Filo del Sol Cu-Au-Ag deposit (lat. 28°29′24″ S, long. 69°39′36″ W) is part of a corridor of porphyry and high-sulfidation epithermal deposits and prospects, informally termed the Filo del Sol alignment, that straddles the international frontier between San Juan Province, Argentina, and Region III, Chile, at elevations between 4,800 and 5,500 m (Fig. 1a, b). Filo Mining Corporation (Filo Mining), listed on the Toronto Stock Exchange and one of the Lundin Group companies, holds a 100% interest in the project, currently the site of a major drilling campaign (www.filo-mining.com).

The ~8.5-km-long, N- to NE-trending Filo del Sol alignment comprises porphyry Cu-Au, Cu-Mo, and related high-sulfidation epithermal Cu-Au-Ag mineralization, with individual centers at Gemelos, Maranceles, La Bonita, El Viejo, Refugio, Ventana, Los Colorados, Vicuña, Tamberías, Flamenco, and Filo del Sol (Fig. 1b). Approximately 12 km northeast of Filo del Sol in San Juan province, Lundin Mining Corporation is currently developing the Josemaría porphyry Cu-Au deposit through its Argentinian subsidiary Desarrollo de Prospectos Mineros S.A. (Deprominsa). In Region III, ~40 km northeast, JX Nippon Mining & Metals exploits the Caserones porphyry Cu deposit through its Chilean subsidiary Minera Lumina Copper Chile, and 15 km northeast, NGEx Minerals Ltd. holds the Los Helados Cu-Au porphyry deposit (Fig. 1b). At Filo del Sol, and the associated Aurora zone in particular, both porphyry Cu-Au and high-sulfidation Cu-Au-Ag styles of mineralization coexist as a large, composite system displaying extreme alteration and mineralization telescoping, i.e., superposition of the two mineralization styles.

Vicuña belt

The Vicuña belt—formalized here for the first time—is a ~40-km-long, NE-oriented corridor of porphyry Cu-Mo, Cu-Au, Au, and high-sulfidation epithermal Cu-Au-Ag deposits and prospects straddling the Argentina-Chile frontier (Fig. 1a, b). The principal deposits along the trend include Filo del Sol

[†]Corresponding author: e-mail, jperello6692@gmail.com
[*]Present address: Irigoyen Hipolito 3615, CABA, Buenos Aires, Argentina.

ISSN 0361-0128; doi:10.5382/econgeo.5029; 30 p.
Digital appendices are available in the online Supplements section.

Submitted: February 7, 2023/Accepted: April 26, 2023

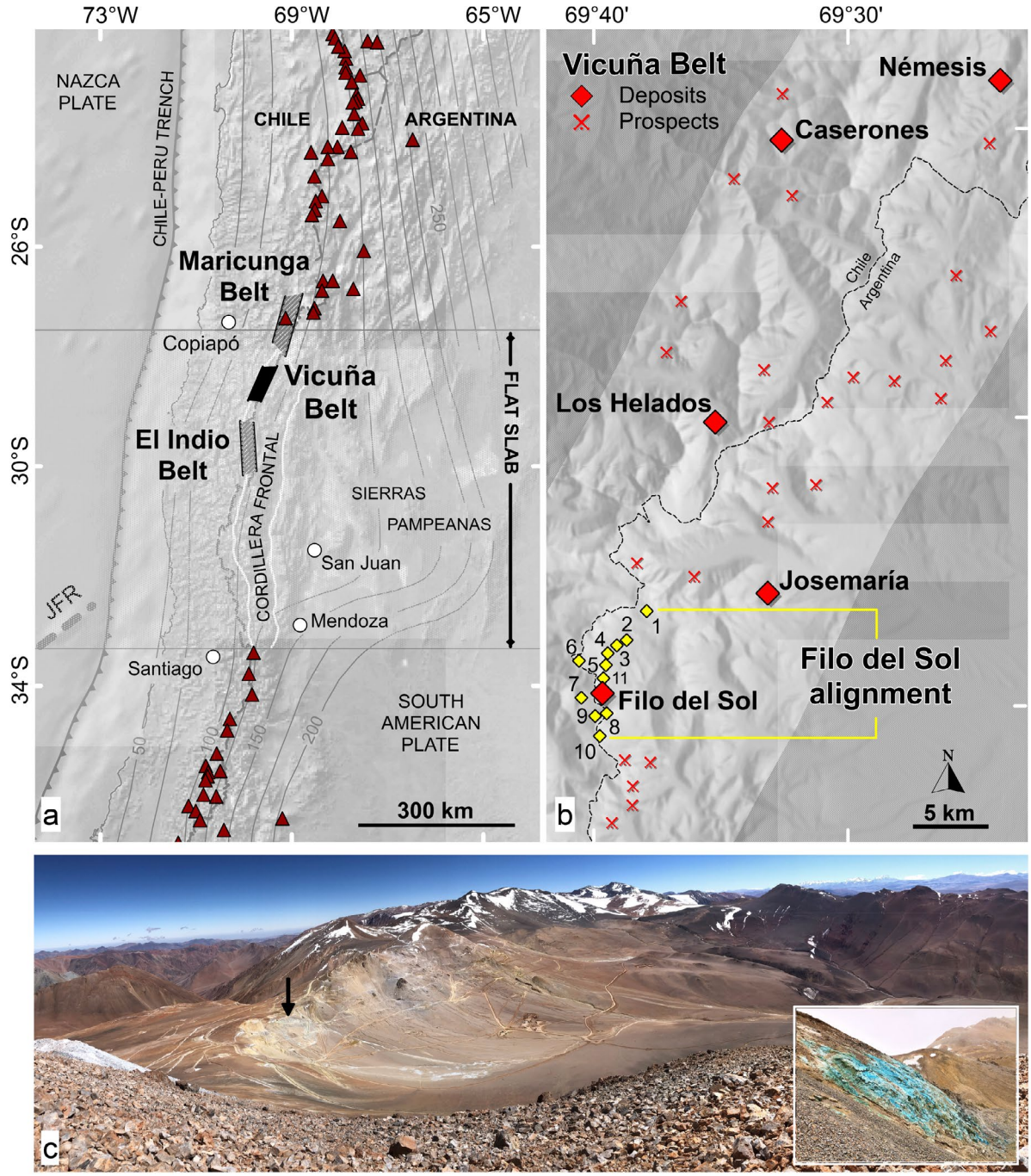

Fig. 1. Regional and local features of the Vicuña belt, Filo del Sol alignment, and Filo del Sol deposit. a. Location of the Vicuña belt between Maricunga and El Indio belts and in relation to the Chilean-Pampean flat-slab segment of subducted Nazca plate (contours from Cahill and Isacks, 1992). Red triangles = active volcanoes, JFR = Juan Fernández ridge. b. Detailed view of the Vicuña belt, as defined herein, with locations of principal deposits and prospects. The Filo del Sol alignment is highlighted. c. General field view of Filo del Sol area, with alteration zone reflecting the lithocap of the Filo del Sol porphyry-epithermal system. Black arrow shows site of Filo del Sol chalcanthite outcrop, which is amplified in inset image. Prospects in Filo del Sol alignment (shown in b): 1. Gemelos, 2. Maranceles, 3. La Bonita, 4. El Viejo, 5. Refugio, 6. Ventana, 7. Los Colorados, 8. Vicuña, 9. Tamberías, 10. Flamenco, 11. Aurora zone.

(this study), Josemaría, Los Helados, and Caserones, with important prospects elsewhere along the Filo del Sol alignment and extensions to the northeast, and in the Caserones area (Fig. 1b). The southern part of the belt is highlighted in satellite imagery by remnants of an initially far larger advanced argillic lithocap in the Filo del Sol area, much of which corresponds to the present-day surface expression of the Aurora zone. Zones of steam-heated alteration are common in the belt, particularly along the Filo del Sol alignment (R.H. Sillitoe, unpub. report, 2010; Devine et al., 2019) and its exten-

sions to the northeast. Magmatism and related mineralization in the Vicuña belt formed during the late Oligocene to middle Miocene (25–14 Ma; Perelló et al., 2003; Yoshie et al., 2015; Devine et al., 2019; Sillitoe et al., 2019; this study), although Permian (266 Ma) porphyry Cu-Mo and Eocene (35 Ma) porphyry Cu-Au mineralization also occurs at El Viejo and Flamenco, respectively (this study; Fig. 1b).

Importantly, the Vicuña belt is located roughly midway between the porphyry and high-sulfidation epithermal deposits of the Maricunga and El Indio belts (Fig. 1a; Sillitoe et al., 1991; Vila and Sillitoe, 1991; Bissig et al., 2001), thereby bridging the metallogenic gap between them.

Objectives and methodology

This preliminary report, prepared in response to the interest generated by spectacular drilling results reported recently from the Aurora zone at Filo del Sol, summarizes the exploration history of the Filo del Sol area, at the southern end of the Vicuña belt, that led to discovery of the Aurora zone; reviews the regional geologic setting; describes the salient geologic and alteration-mineralization features of Filo del Sol; documents the timing of magmatic and hydrothermal events in the Filo del Sol area; and outlines the geologic evolution of the telescoped porphyry and high-sulfidation mineralization at Filo del Sol in a regional tectonomagmatic context. The report is based on geologic work by the writers and other Lundin Group geologists during several exploration phases over a period of 22 years, and incorporates data from previously published descriptions and studies of the Filo del Sol area (Devine et al., 2017, 2019; Charchaflié et al., 2019) and vicinity (Sillitoe et al., 2019).

To accomplish these aims, detailed mapping of lithology, structure, and alteration was conducted at various scales over most of the Filo del Sol alignment (Fig. 1b). Subsurface geology is based on logging of ~43,000 m of core from 88 drill holes and 26,000 m of cuttings from 90 reverse-circulation drill holes, leading to construction of 17 hand-drawn geologic and alteration cross sections at 1:2,000 scale, which encompass ~1.6 km of strike. Hydrothermal alteration is modeled on the basis of detailed logging complemented by petrographic work and short-wave infrared (SWIR) reflectance spectroscopy. SWIR data are routinely collected at 2-m intervals on drill core and cuttings with an ASD TerraSpec IR spectrometer. The U-Pb zircon and Re-Os molybdenite geochronologic data reported here (17 U-Pb zircon and 22 Re-Os molybdenite ages) follow conventional protocols, methods, and operating procedures. Further description of the methodology, equipment, isotopic data, and reference materials are provided in Appendices 1 and 2, respectively.

Exploration History

The Lundin Group, through various subsidiary companies, has been engaged in exploration of the region between the Maricunga and El Indio belts since the 1990s (Jones, 2007; Jones and Martínez, 2007; Rode and Carrizo, 2007). Initial exploration used LANDSAT TM false-color imagery to rapidly detect and secure mineral rights over color anomalies with potential to host mineralization (Rode and Carrizo, 2007). Field validation of the color anomalies combined with geochemical sampling and mapping quickly identified several exploration targets in the Vicuña belt (Figs. 1b, 2). These efforts, coupled with persistent, long-term follow-up work, resulted in discovery of the shallow oxide mineralization at Filo del Sol in 2001, Josemaría in 2004, Los Helados in 2008, and the deeper, high-grade Aurora porphyry-epithermal zone in 2020.

Attracted by abundant Cu showings, the first documented company to conduct formal exploration in the Filo del Sol area was Cyprus-Amax in 1997, mainly in the Chilean part of the Vicuña prospect (Fig. 1b). Cyprus-Amax conducted 1:10,000-scale geologic mapping, systematic grid sampling of talus-fines, selective rock-chip sampling, and 2,519 m of reverse-circulation drilling in 16 shallow holes (Fig. 2a). The drill holes intersected spatially restricted, high-grade Cu oxide and moderately anomalous Au values within a large talus-fines Au anomaly. Cyprus-Amax geologists correctly identified banded quartz veinlets like those first recognized in porphyry Au deposits of the Maricunga belt by Vila and Sillitoe (1991), which may have led to downgrading of Vicuña's Cu potential. In mid-1999, a purchase agreement was reached with Tenke Mining Corporation (Tenke), one of the early Lundin Group companies established to explore the area. Simultaneously, Tenke negotiated contiguous Argentinian properties with local owners, thereby consolidating 100% of the mineral rights on both sides of the international frontier. During the summer seasons of 1999 and 2000, Tenke geologists carried out geologic mapping at 1:20,000 and 1:5,000 scales, grid sampling of talus-fines, trenching, and geophysics. The geophysical work comprised magnetic, induced polarization (IP), and magnetotelluric (CSAMT) surveys. In 2000 and 2001, the Filo del Sol area was optioned to Rio Tinto, with Tenke´s local subsidiary, Deprominsa, being the operator. Approximately 4,000 m of scout reverse-circulation drilling was completed, following which Rio Tinto terminated the option agreement.

An exploration joint-venture with Japan Oil, Gas and Metals National Corporation (JOGMEC) was active between 2004 and 2012 over the entire Vicuña belt land package. Due to positive exploration results at Josemaría and Los Helados (e.g., Rode et al., 2015; Sillitoe et al., 2019), little systematic work was conducted in the Filo del Sol area, although several short drilling programs tested specific targets and concepts. Approximately 6,300 m of reverse-circulation drilling and the first, short (280 m) core hole, were completed (Fig. 2a). Importantly, in 2006, the Filo del Sol project area was granted Additional Protocol status (the Vicuña Mining Prospection Project) as part of the Mining Integration and Complementation Treaty between Chile and Argentina, thereby allowing exploration to be conducted on both sides of the international frontier. In 2009, Deprominsa became part of NGEx Resources Ltd. (NGEx), a new Canadian-listed public company in the Lundin Group. Exploration at Filo del Sol resumed slowly in 2011 and accelerated in 2013 and 2014, when 8,400 m in 24 reverse-circulation holes and two core holes were drilled (Fig. 2b). Semiregional geologic mapping was initiated during the 2014–2015 summer season to provide a geologic, chronologic, and tectonic framework for the project (F. Devine et al., unpub. report, 2015; Devine et al., 2016). The drilling results underpinned successive resource estimates released between 2014 and 2015 (Charchaflié and Gray, 2014; Devine et al., 2015), prior to Filo Mining Corporation being spun off from NGEx in 2016, thereby allowing the new company to focus on

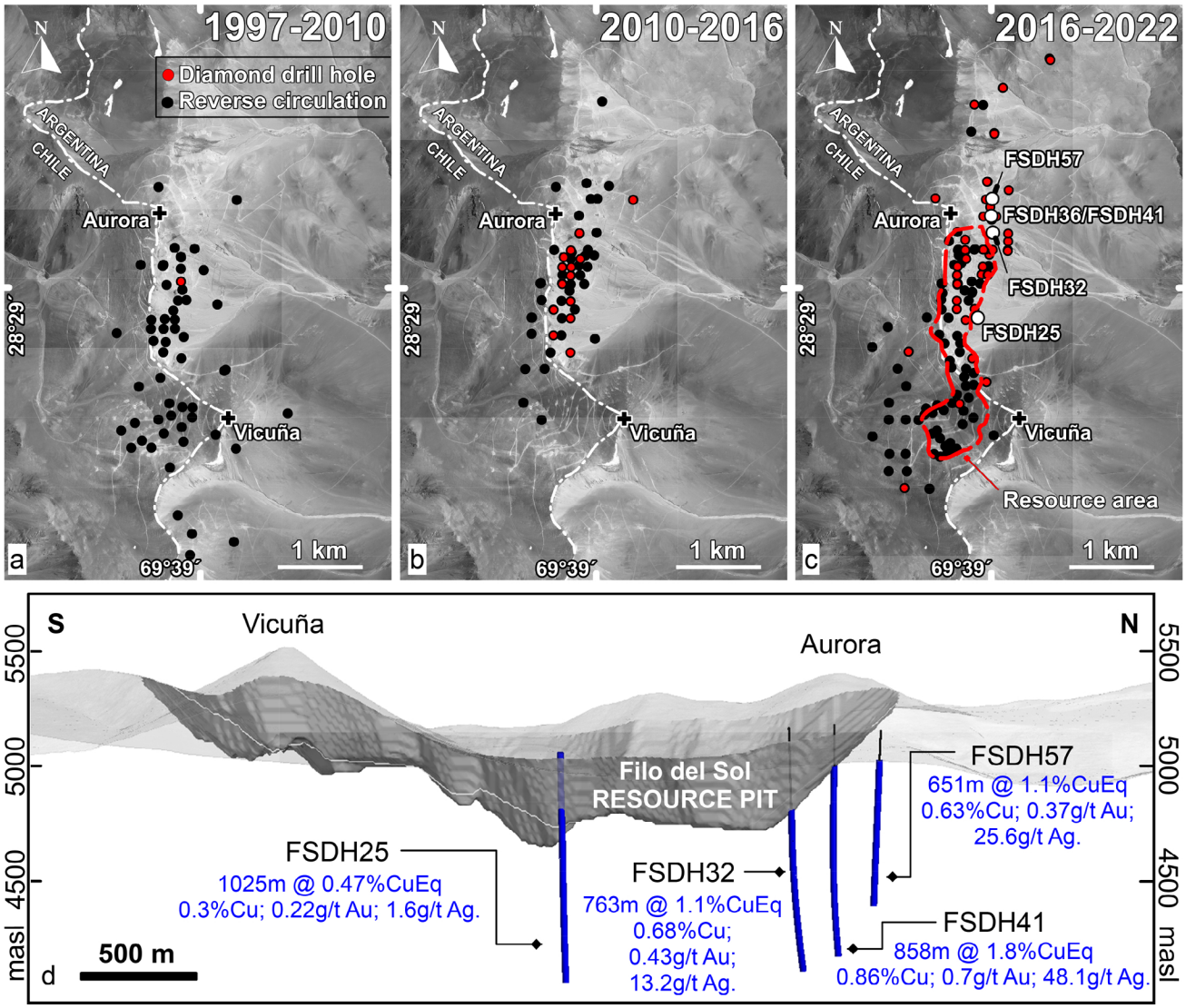

Fig. 2. Summary exploration history of Filo del Sol deposit. a–c. Three scenes showing drilling campaigns from 1997 to 2022, with emphasis on key core holes leading to discovery of the Aurora zone. The resource area of the shallow, leachable Filo del Sol deposit is also shown. d. Long section (S to N) of Filo del Sol area, showing principal drill holes and mineralized intercepts of the Aurora Cu-Au-Ag zone.

the Filo del Sol area. Reverse-circulation and diamond drilling intensified during the 2017 and 2018 seasons (Fig. 2c), leading to a preliminary economic assessment of the shallow oxide part of the Filo del Sol deposit (Devine et al., 2017). In early 2019, a prefeasibility study concluded that the shallow Filo del Sol deposit (Fig. 2c) contained an indicated mineral resource of 349.6 Mt of oxide mineralization at 0.34 % Cu, 0.32 g/t Au, and 12.6 g/t Ag at a 0.15% Cu-equivalent (CuEq) cutoff, and 75.5 Mt of sulfide mineralization at 0.27 % Cu, 0.34 g/t Au, and 2.2 g/t Ag at a 0.3% CuEq cutoff (Devine et al., 2019). Soon after release of the prefeasibility report, Filo Mining decided to continue exploring beyond and below the Filo del Sol resource rather than advance it to the feasibility stage.

During the 2018–2019 exploration season, seven deep diamond drill holes to test potential beneath the Filo de Sol resource shell were attempted and partially completed. Hole FSDH25 (Fig. 2c, d), the first exceeding 1 km in depth, intersected moderate Cu and Au grades hosted by potassic-altered porphyry and a large body of magmatic-hydrothermal breccia, both overprinted by steep zones of highly silicic advanced argillic alteration and associated high sulfidation-state Cu sulfides and Cu-As sulfosalts (R.H. Sillitoe, unpub. report, 2019). The hole was the first to encounter a deep, potassic-altered, porphyry Cu-bearing intrusion north of the Vicuña prospect (Fig. 2c, d), confirming previous suggestions by the exploration team in 2003–2004 and documented predictions (R.H. Sillitoe, unpub. reports, 2001, 2010).

In parallel with the drilling, data from historic geophysical and SWIR surveys were reassessed and, combined with new geologic mapping, resulted in modification of the structural and alteration interpretations of the area (D. Charchaflié, unpub. report, 2018; J. Rossello and J. Arrieta, unpub. report, 2018; W.F. Kerby, unpub. report, 2018). The results

highlighted a dominant N to NE trend of the alteration zone which, together with new data on pathfinder elements, defined a northward vector toward more intense quartz-alunite alteration and potential for associated high-sulfidation mineralization at Aurora (D. Heberlein, unpub. report, 2015; Charchaflié et al., 2019; J. Rossello and M. Sanguinetti, unpub. report, 2019), in keeping with the predicted existence of deep northward extensions to the system based on drill-core observations (R.H. Sillitoe, unpub. report, 2019). The concept was tested in 2020 by hole FSDH32 (Fig. 2c, d), a twin of a 270-m reverse-circulation hole completed in 2015, which intercepted 763 m averaging 1.1% CuEq (Fig. 2d) as predominantly high-sulfidation mineralization. Drilling continued with great difficulty under strict protocols during the Covid-19 pandemic in 2020 and 2021, when the site of FSDH36 was redrilled and, after numerous attempts due to poor ground conditions, FSDH41—considered as the Aurora zone discovery hole—intersected 858 m at 1.80% CuEq (Fig. 2c, d). Intervals with bonanza-grade Cu, Au, and Ag values (e.g., 163 m at 5.43% CuEq) coincide with high-sulfidation mineralization hosted by a zone of vuggy residual quartz and associated quartz-alunite alteration. FSDH57, drilled in 2022, confirmed the northward continuation of the bonanza-grade mineralization (Fig. 2c, d).

Current status

Filo Mining is currently engaged in an aggressive drilling program designed to determine the high-grade resource at Aurora and overall size of the porphyry and high-sulfidation epithermal system in the greater Filo del Sol deposit. The large footprint of the alteration-mineralization suggests that the system has the potential to host a deposit containing >1,000 Mt at >0.7% CuEq.

Regional Geologic Setting

The ~40-km-long portion of the southern Central Andean Cordillera between latitudes 28°11′ and 28°32′ S, defined here as the Vicuña belt, is part of a much larger, N-trending, late Oligocene to middle Miocene magmatic arc that straddles the northern boundary of the present-day Chilean-Pampean flat-slab segment (~27°–33° S; Jordan et al., 1983; Cahill and Isacks, 1992; Kay and Mpodozis, 2002; Anderson et al., 2007; Fig. 1a). The Maricunga belt that lies to the north contains numerous porphyry Au, porphyry Au-Cu, and high-sulfidation epithermal Ag-Au deposits (Sillitoe et al., 1991; Vila and Sillitoe, 1991; Kay et al., 1994; Mpodozis et al., 1995; Muntean and Einaudi, 2001), and the El Indio belt to the south is dominated by high-sulfidation epithermal Au-Ag and Cu-Au deposits (Jannas et al., 1999; Bissig et al., 2001; Chouinard et al., 2005; Charchaflié et al., 2007; Holley et al., 2016). In both the Maricunga and El Indio belts, Oligocene to early Miocene volcanic rocks are widespread and include numerous volcanic landforms, some coeval with mineralization. In contrast, the higher altitude Filo del Sol area has only sparse, structurally localized volcanic cover, believed to be due mainly to its erosional removal (Mpodozis and Kay, 2003; Martínez et al., 2015b; Salazar and Coloma, 2016; Rossel et al., 2018).

The regional geology of the Vicuña belt (Fig. 3a) is dominated by fault-bounded blocks of Permo-Triassic volcano-plutonic rocks, including multiphase granitoid batholiths (e.g., Nasi et al., 1985) that either intrude or are unconformably overlain by felsic volcanic sequences. The latter range from ~284 to 228 Ma in age, based on numerous U-Pb determinations for exposures on the Chilean side of the frontier (Martínez et al., 2015a; Salazar and Coloma, 2016), whereas the granitoid intrusions were mainly emplaced between ~285 and 247 Ma (Maksaev et al., 2014; Martínez et al., 2015a, b; Salazar and Coloma, 2016; del Rey et al., 2019). These igneous rocks are assigned to the Choiyoi large igneous province (also, Choiyoi magmatic province; Kay et al., 1989; Sato et al., 2015; Bastías-Mercado et al., 2020; Gianni and Navarrete, 2022) that extends from northern Chile through the Frontal Cordillera of Argentina and Chile and southward as far as Argentinian Patagonia (Sato et al., 2015).

Mesozoic volcano-sedimentary rocks, which unconformably overlie the older sequence, are preserved as tectonic wedges between uplifted basement blocks (Moscoso and Mpodozis, 1988; Martínez et al., 2015a, b, 2016, 2018; Salazar and Coloma, 2016); they include a basal marine sequence of calcareous shale and limestone of Early Jurassic age overlain by continental siliciclastic strata with local volcanic intercalations of Late Jurassic to early Paleogene age (Martínez et al., 2015a; Salazar and Coloma, 2016). Continental volcanic rocks and associated terrigenous strata of late Eocene to early Miocene age are preserved only locally on the Chilean side of the frontier (Martínez et al., 2015a; Salazar and Coloma, 2016), but are more widespread farther east in Argentina, where they occupy structurally defined basins (Fig. 3a, b; Panteleyev and Cravero, 2001; Sillitoe et al., 2019). With the exception of a few restricted and isolated outcrops of middle Miocene age, the nearest ~40 km southwest in Chile (Salazar and Coloma, 2016), the Vicuña belt lacks any vestiges of 15 to 13-Ma volcanic activity that is widespread to the north and south along the Maricunga and El Indio belts, respectively (Kay et al., 1994; Bissig et al., 2001). However, small Eocene to Miocene intrusions are present throughout the Vicuña belt.

Extensive removal of the Oligocene to early Miocene volcanic cover occurred in response to the kilometer-scale uplift of Permo-Triassic basement-cored blocks on major N- to NE-trending reverse faults that led to construction of the Frontal Cordillera (Moscoso and Mpodozis, 1988; Martínez et al., 2015a, b; Salazar and Coloma, 2016; Mpodozis et al., 2018). Regionally, these structures include the El Potro fault in Chile (Martínez et al., 2015a; Salazar and Coloma, 2016; Rossel et al., 2018) and the Mogotes fault system in Argentina (Fig. 3a, b). Diachronous displacement along the El Potro and other reverse faults in the Chilean Frontal Cordillera commenced in the early Miocene (~21–19 Ma; Martínez et al., 2015a, b; Rossel et al., 2018), broadly contemporaneous with initial subducted slab flattening (~20–18 Ma; Kay et al., 1994; Kay and Mpodozis, 2001). The easternmost faults in Chile, near the international border, were active in the middle Miocene (~13 Ma: Rossel et al., 2018). Farther south, at the latitude of El Indio, equivalent compressive tectonism occurred at ~14 Ma (Maksaev et al., 1984; Martin et al., 1997; Giambiagi et al., 2017, 2022), with erosion and pediment formation active between 14 and 12.5 Ma (Bissig et al., 2002). At the same latitude in the Valle del Cura region of Argentina, however, tectonic inversion commenced between 20 and 18 Ma and may have continued to ~13 Ma (Winocur et al., 2015).

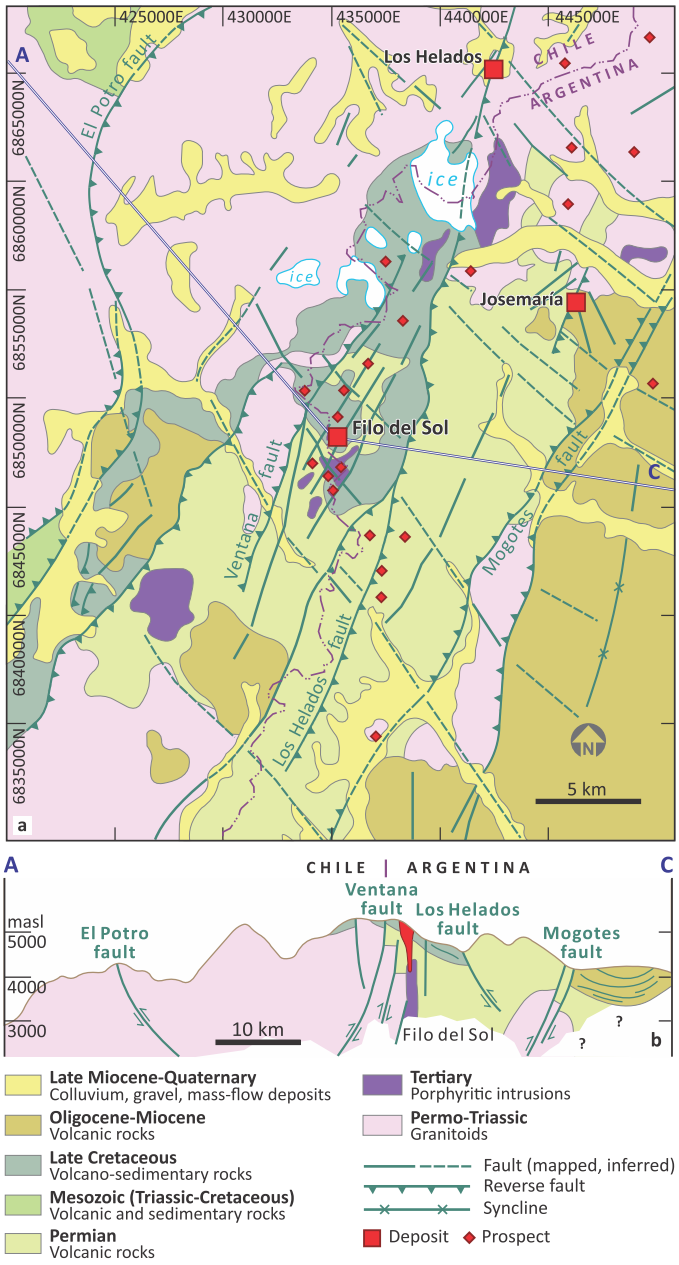

Fig. 3. Geologic setting of Filo del Sol alignment. a. Regional geologic map, based on Martínez et al. (2015a) and Salazar and Coloma (2016), for Chilean territory, and project work, Devine et al. (2019), and Sillitoe et al. (2019) for Argentinian territory. UTM projection WGS84-zone 19. b. Schematic cross section of the region, prepared by the project team, showing location of Filo del Sol system. Several structural and geologic elements in Chilean territory adapted from Martínez et al. (2015b). Vertical exaggeration ×2.5.

The Vicuña belt and its northward and southward transitions to the Maricunga and El Indio belts, respectively, span the northern limit of the flat-slab segment (Fig. 1a). Porphyry and epithermal deposits and prospects formed in several pulses during the late Oligocene and Miocene, both before and during slab shallowing and concomitant crustal thickening. Gold-bearing porphyry Cu deposits at Caspiche (26 Ma; Sillitoe et al., 2013) and Josemaría (25 Ma; Sillitoe et al., 2019), together with several prospects in the Caserones area (~26–23 Ma; Perelló et al., 2003; Yoshie et al., 2016), formed prior to slab shallowing, whereas the Caserones Cu-Mo (19–17 Ma; Yoshie et al., 2015) and Los Helados Cu-Au (~14 Ma; Guitart, 2020) deposits are examples of porphyry deposits contemporaneous with slab flattening. Magmatism and Cu-Au-Ag mineralization throughout the Filo del Sol alignment took place during slab flattening at ~15 to 14 Ma (see below). Approximately 80 km farther south, at the northern extremity of the El Indio belt at ~29°S, porphyry Cu-Au mineralization at Valeriano and Encierro was active at 11 to 10 Ma (Sillitoe et al., 2016; J. Perelló, unpub. data, 2016), broadly simultaneous with the Veladero (~12–10 Ma) and before formation of the Pascua-Lama (9–8 Ma) high-sulfidation epithermal Au deposits (Bissig et al., 2001; Charchaflié et al., 2007; Holley et al., 2016). Together, these deposits demonstrate metallogenic continuity between the Vicuña, Maricunga, and El Indio belts, a concept anticipated two decades earlier (Mpodozis and Kay, 2003; Sillitoe and Perelló, 2005; Fig. 1a).

Filo del Sol Geology

Country rocks

The Filo del Sol porphyry-epithermal Cu-Au-Ag system is spatially and genetically related to a composite, N- to NE-trending swarm of biotite- and hornblende-bearing porphyry dikes of broadly dioritic composition emplaced into Permo-Triassic basement units and Late Cretaceous volcano-sedimentary rocks (Figs. 3–5). A series of mafic dikes, characteristically of microdioritic composition and texture, follow the same trend. The Permo-Triassic units of Choiyoi affiliation comprise felsic volcanic and volcaniclastic rocks and a granitoid intrusion. Massive to thickly bedded, locally flow-banded volcanic and subvolcanic rocks, including airfall tuff, ignimbrite, volcanic breccia, and lava flows, are all predominantly rhyolitic to rhyodacitic in composition; porphyritic and fragmental textures are prevalent. Where fragmental, 20 to 40 vol % of centimeter-sized vitreous, crystal, and lithic clasts occur in various proportions, with compaction foliation recognizable locally. The Filo del Sol granitoid body, mainly leucocratic monzogranite, is characterized by coarse-grained, porphyritic to inequigranular texture and perthitic intergrowths of quartz and K-feldspar and abundant graphic texture. Fine-grained intrusive variants include dikes and irregular pods of aplite and microgranite, typically present near or at contacts with the host volcanic rocks. On the basis of U-Pb zircon dating, the felsic volcanic rocks are assigned a middle Permian to earliest Triassic age, with the crosscutting monzogranite being Middle Triassic (Table 1).

The Permo-Triassic units in much of the Vicuña belt are unconformably overlain by massive to thickly bedded, terrigenous sedimentary and volcanic rocks. At Filo del Sol, the sequence forms an open, NE-trending syncline with ~20° E- and W-dipping limbs, although in contiguous Chile it is more steeply W-dipping. A basement-cored anticline, similar to those common in neighboring Chile, is inferred (Martínez et al., 2015a, b; Fig. 3b). The lower, red-bed part of the sequence consists of massive to thickly bedded, poorly sorted, normal- and reverse-graded horizons of pebbly to blocky conglomerate and thickly bedded lithic sandstone, interbedded with irregular andesite flows, sills, and volcaniclastic material.

Table 1. Summary LA-ICP-MS U-Pb Age Data for Filo del Sol Alignment

Sample	UTM[1] N/E	Age, Ma	Comments
FSDH046-1093	6848991/435597	15.6 + 0.4/–0.3	Early-intermineral porphyry, Aurora zone
FSDH025-773	6848000/435247	15.2 ± 0.5	Early-intermineral porphyry, Filo del Sol
FSDH32A-752	6849002/435416	15.0 + 0.3/–0.4	Early-intermineral porphyry, Filo del Sol
FSDH43-396	6850160/435427	15.6 ± 0.4	Intermineral porphyry, Refugio
FSDH046-1452	6848991/ 435597	15.2 + 0.3/–0.2	Late-intermineral porphyry, Aurora zone
15FD872[2]	6848752/434914	15.475 ± 0.042	Late-intermineral porphyry, Aurora zone
FSDH034C-1038	6850160/435427	231.8 ± 3.2	Monzogranite, Filo del Sol
FSDATA05	6849838/435042	250.6 ± 1.5	Felsic sequence, Filo del Sol area
FSDATA07	6851840/437127	253.0 ± 2.7	Felsic sequence, Filo del Sol area
FSDATA08	6850335/436890	259.3 ± 1.0	Felsic sequence, Filo del Sol area
FSDATA25	6846636/433251	268.7 ± 2.6	Felsic sequence, Filo del Sol area
FSDH34C-623	6848506/435362	255 ± 3.6	Felsic sequence, Filo del Sol area
FSDATA24	6847663/436533	67.5 ± 0.4	Volcano-sedimentary sequence, Vicuña
FSDATA12	6847797/436388	75.2 ± 0.9	Volcano-sedimentary sequence, Vicuña
FSDATA16	6845183/433961	37.0 ± 1.3	Mafic dike, Filo del Sol area
FSDH21-10	6848100/434993	81.9 ± 0.7	Mafic dike, Filo del Sol area
FSDH54-24	6849192/435455	15.8 + 0.2/–0.3	Mafic dike (precursor?), Aurora zone

See Appendix 1 for additional zircon analytical data; LA-ICP-MS = laser ablation-inductively coupled plasma-mass spectrometry

[1] UTM projection WGS84-zone 19

[2] Dated by the isotope dilution-thermal ionization mass spectrometry (ID-TIMS) method

The basal section in contact with Permo-Triassic rocks, immediately east of Filo del Sol, is dominated by meter-sized blocks and smaller fragments of rhyolitic composition (Fig. 6a). Upper parts of the sequence are mainly massive flows and sills of dark porphyritic andesite. The overall thickness of the sequence is highly variable in the Filo del Sol area, from just a few to hundreds of meters, with thicker sections likely confined to structurally controlled depressions over an irregular paleosurface. This sequence can be correlated with similar, mostly Mesozoic-age rocks in Chile (Martínez et al., 2015a; Salazar and Coloma, 2016). On the basis of detrital and magmatic U-Pb zircon dating in the Filo del Sol area, these rocks are assigned a Late Cretaceous age (Table 1).

North- to NE-trending mafic dikes and associated sills in the Filo del Sol area vary in texture and composition from porphyritic, amygdaloidal andesite to massive microdiorite (Fig. 6b, c). Where less altered, the dikes are dark gray to black, with plagioclase, hornblende, biotite, and magnetite as dominant components. Large dikes occur along the eastern and western sides of the entire deposit, and several sills intruded at the contact between the Permian volcanic rocks and overlying Cretaceous sequence and within the latter unit. One large sill, ~200 m thick, is preserved in the southern part of the deposit, effectively capping the later porphyry Cu-related dikes and associated breccias (Fig. 5b). The dikes and sills are clearly post-Cretaceous, although some intruded into wet sediment judging by the chaotic forms of contacts and local peperitic texture. Although most of the mafic intrusions are pre-Miocene in timing, in accord with their U-Pb zircon ages, one potassic-altered dike in the Aurora zone reported a middle Miocene U-Pb zircon age (Table 1), suggesting that it may be a precursor to the porphyry Cu-related intrusions in the Filo del Sol deposit.

Porphyry intrusions

Three principal porphyry phases are distinguished at Filo del Sol and assigned to two families: early- and late-intermineral. Phases 1 and 2 are grouped together as the early-intermineral family, whereas phase 3 constitutes the main late-intermineral intrusion. Both families constitute a dike swarm, >1.5 km in vertical extent and at least 2 km along strike, that are coincident with the north to northeast trend of the Filo del Sol alignment. The relative ages of porphyry intrusions are determined using conventional geologic criteria (e.g., Sillitoe, 2000, 2010; Proffett, 2003): intrusive contact relationships, quartz-veinlet intensity, veinlet truncation at contacts, refractory quartz-veinlet xenoliths in younger phases, and Cu and Au contents. The earliest, phase 1 intrusion (Fig. 6d) is preserved mainly as bodies of varied dimensions, some entirely enclosed by phase 2. In the central parts of the swarm, the main porphyry is phase 2, occurring as dikes tightly confined to a ~500-m-wide corridor (Fig. 5).

Early-intermineral porphyry dikes are characterized by crowded, medium- to coarse-grained (up to 6 mm), seriate, porphyritic texture, with ~15 to 40 vol % phenocrysts of plagioclase, biotite, and amphibole, in addition to minor amounts of quartz (Fig. 6d, e). Plagioclase phenocrysts are tabular and zoned, biotite is idiomorphic—typically as books, amphibole is prismatic, and quartz is normally anhedral and resorbed, with local quartz eyes. Groundmass, typically more abundant in the later phases, is fine-grained to aphanitic. Late-intermineral porphyry intrusions are typically medium-grained, porphyritic and have a greater proportion of aphanitic groundmass, although coarser-grained textures also appear at depth (Fig. 6f). All the porphyry intrusions, including phase 3, were originally characterized by K-feldspar-biotite-bearing potassic alteration. Postmineral porphyry intrusions were not observed at Filo del Sol or in nearby areas.

The porphyry intrusions are middle Miocene (16–14 Ma) in age, as constrained by several U-Pb zircon dates from Aurora (this study) and elsewhere within and adjacent to the Filo del Sol area (e.g., Devine et al., 2019; Table 1).

Early magmatic-hydrothermal breccia

A large magmatic-hydrothermal breccia body accompanies the early-intermineral porphyry dike swarm at Filo del Sol

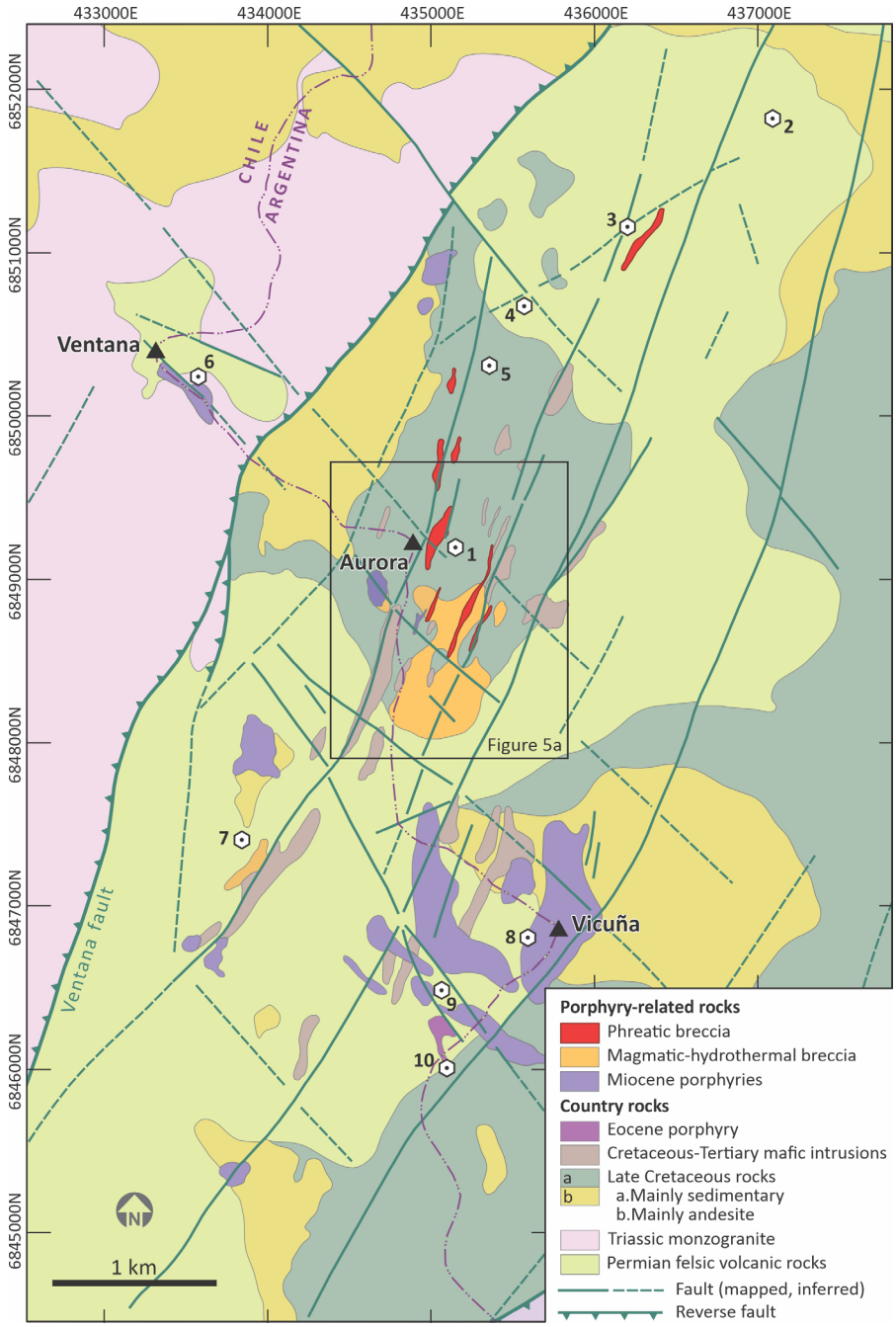

Fig. 4. Geologic map of Filo del Sol alignment, based on work by the authors. Note surface expression of magmatic-hydrothermal breccia at the Aurora zone and dominant north to northeast trend of geologic features at Filo del Sol, including premineral mafic dikes, late-mineral phreatic breccias, and principal postmineral faults. Also note northwest trend of porphyry-related intrusions at Tamberías and Flamenco. Inset shows locations of Aurora zone as in Figure 5a. Key to deposits and prospects: 1. Filo del Sol 2. Maranceles, 3. La Bonita, 4. El Viejo, 5. Refugio, 6. Ventana, 7. Los Colorados, 8. Vicuña, 9. Tamberías, 10. Flamenco.

(Figs. 4, 5). The breccia is mainly polymictic and clast supported, with the main body ~500 m wide and 1,300 m in vertical extent (Fig. 5). It contains clasts of country rock, including porphyritic and fragmental rhyolite, granite, microdiorite, andesite, and volcaniclastic rocks, as well as porphyry Cu clasts. Angular to subrounded, pebble-sized fragments dominate, although larger blocks, some apparently several tens of meters in diameter, are inferred from extended drill-core intercepts. The breccia typically contains fragments of A-type quartz veinlets (sensu Gustafson and Hunt, 1975) and is cut by later generations of similar veinlets (Fig. 6g, h). Fine-grained, aplitic cement, composed of intergrown quartz and K-feldspar, is present at depth, and pegmatoidal facies composed of K-feldspar, biotite, and anhydrite aggregates, with individual crystals

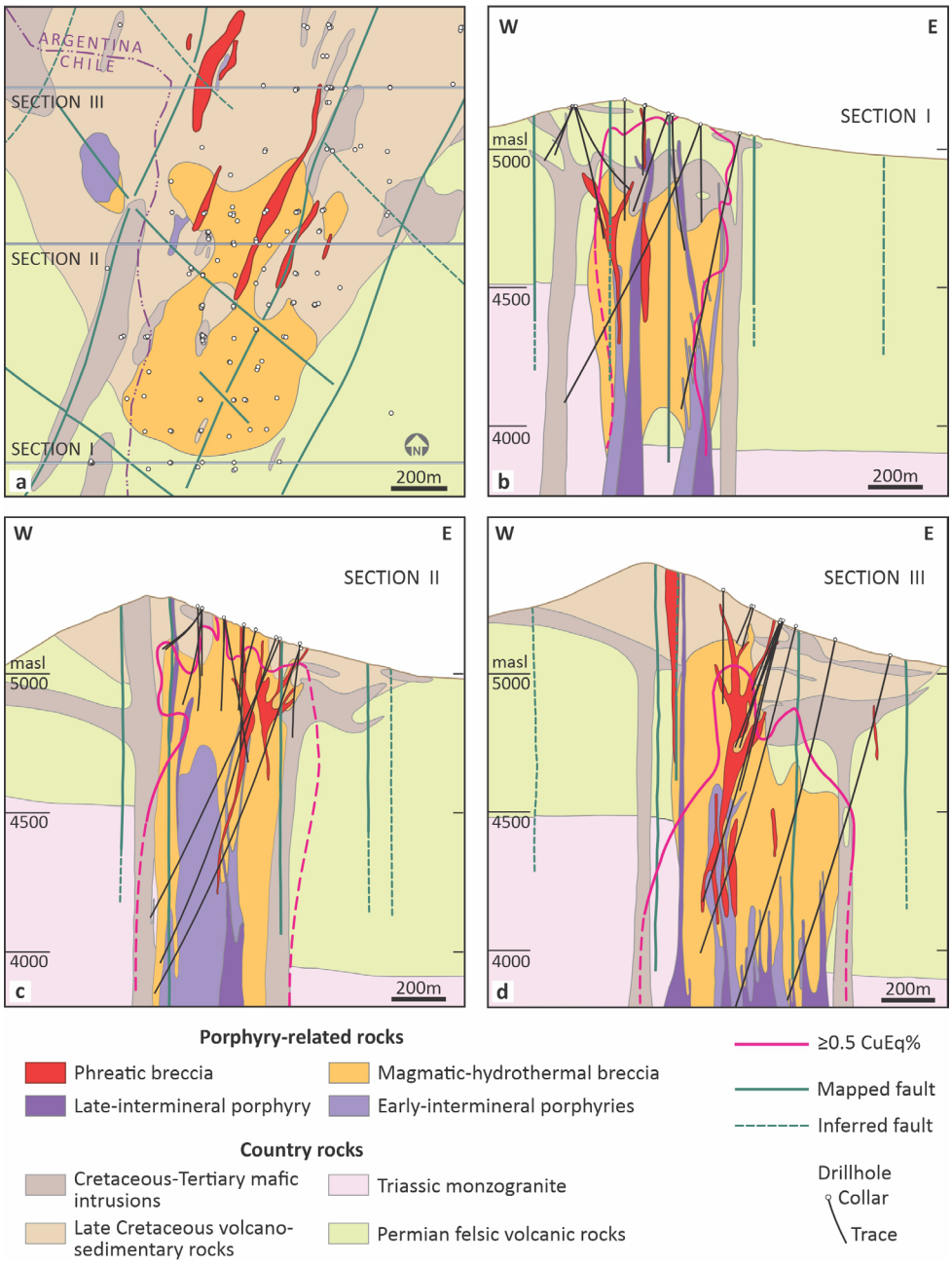

Fig. 5. Geology of Filo del Sol deposit. a. Plan view showing location of cross sections in b–d. See Figure 4 for location. b–d. Sections I, II, and III, prepared with a 50-m clipping, displaying principal geologic features of the deposit. Note two subparallel mafic dikes in all sections, overlying sill in section I, and additional sills at contact between Permian felsic volcanic and Late Cretaceous volcano-sedimentary sequences. Also note vertical step in contact between Triassic monzogranite and overlying Permian volcanics rocks, inferred to be a steep, N- to NE-trending, premineral fault that influenced location of Filo del Sol porphyry system. See text for additional discussion. The >0.5% Cu-equivalent (CuEq) shell is shown for reference. Copper equivalent for drill intersections is calculated based on US$3.00/lb Cu, US$1,500/oz Au, and US$18/oz Ag, with 80% metallurgical recoveries assumed for all metals. The formula is: CuEq % = Cu % + (0.7292 · Au g/t) + (0.0088 · Ag g/t). See www.filo-mining.com.

up to several centimeters in size, also occur locally (Fig. 6i). A variety of pegmatoidal breccia contains tabular bodies of coarse-grained, crystalline, and massive anhydrite up to tens of meters in size.

Breccia clasts, including larger blocks, are characteristically rotated and displaced relative to one another, but underwent only minor vertical displacement; as such, throughgoing geologic contacts can be reliably inferred. Although the breccia is largely composed of basement rhyolite fragments, there is an apparent zoning, with porphyry and rhyolite dominant internally and other lithologies progressively more abundant both laterally and upward. A tendency for clasts to become smaller upward in the breccia body is also apparent, as is the presence of thin, fine-grained quartz-veinlet fragments in its shallow-

est parts. In common with its associated porphyry phases, the breccia was originally emplaced under potassic-stable conditions, and is inferred to have been formed by overpressured magmatic fluid released from an underlying intermineral magma body (cf. Sillitoe, 1985, 2010, and references therein). At Filo del Sol, the breccia is the main host not only for the early porphyry-related Cu-Au mineralization, but also for the bulk of the overprinted high-sulfidation Cu-Au-Ag mineralization.

Late hydrothermal breccia

Several hydrothermal breccia dikes occur at Filo del Sol, the largest of which is ~500 m long and ~80 m wide; these breccia dikes accompany the mineralized porphyry dikes and magmatic-hydrothermal breccia, and follow the principal north to northeast trend (Figs. 4, 5). The breccia occurs mainly in shallow parts of the system at elevations of 4,800 to 5,000 m, with several restricted bodies exposed at surface; however, breccia dikes are recognized to depths of ~1,000 m (Figs. 4, 5). This late hydrothermal breccia is represented by several distinct bodies and types, the most abundant inferred to be of phreatic origin; however, other important varieties have sulfate and/or sulfide cements, tuffaceous matrix with juvenile quartz, plagioclase, and biotite crystal fragments as well as local wispy injections of banded feldspar porphyry, all indicative of a phreatomagmatic origin.

The main phreatic breccia body is polymictic, poorly sorted, and matrix supported. It is typically composed of ~30 vol % of subangular to subrounded clasts, up to several centimeters in diameter, comprising felsic volcanic, porphyry, and devitrified rock; characteristically, this phreatic breccia contains abundant A-type quartz-veinlet clasts (Fig. 6j, k). The clastic matrix is fine grained (rock flour in places and cloudy in thin section), nonbedded, and loosely aggregated; randomly distributed, millimeter-sized particles of quartz and lithics of composition similar to the clasts are present. Some larger fragments appear polished, but sphericity is uncommon. The matrix is typically impregnated with hydrothermal minerals, including alunite, kaolinite, pyrite, and Cu-As sulfosalts. Besides the numerous quartz-veinlet fragments, the breccia also contains clasts that display alunite-rich, advanced argillic alteration plus residual quartz with vuggy texture and silicified rock; importantly, the phreatic breccia is nowhere cut by quartz veinlets, confirming its formation during the advanced argillic alteration event. At shallow levels, the breccia transects the Late Cretaceous sedimentary sequence and, where exposed at surface (Fig. 4), the clasts it hosts are key indicators of porphyry-type veining and mineralization at depth.

The late breccia is cut by younger generations of steeply inclined breccia dikes, typically a few meters wide; they are commonly characterized by fine-grained, thinly bedded to laminated, tuffaceous material, displaying both low-angle crossbedding and convolute laminations (Fig. 6l) that are described in petrographic studies as surge-type textures. In places, the laminations are also subparallel to the breccia contacts, suggestive of upward-streaming or, perhaps, fluidization processes (McCallum, 1985). Many of these dikes contain disseminated sulfides, whereas others clearly acted as fluid conduits based on subsequent deposition of sulfate (anhydrite, alunite) and sulfide (pyrite, Cu-As sulfosalts) minerals.

Hypogene Alteration and Mineralization Features

Two principal alteration types are recognized and routinely modeled at Filo del Sol: early, deep potassic, and late, shallow advanced argillic, with the latter overprinting the former. An intervening zone of quartz and fine-grained white mica (sericite) overprints potassic alteration in the central parts of the deposit but becomes more widespread and better developed both laterally and along strike toward the northern and southern extremities of the system. In addition to these two main alteration types at Filo del Sol, the uppermost parts of the lithocap underwent intense steam-heated alteration. Defining an extensive propylitic halo at surface, chlorite-epidote alteration fringes the system on both sides of the international frontier (Fig. 7). In the project area, however, only the internal portion of this halo, dominated by a mixture of chlorite, white mica, and remnant biotite, occurs at the surface and, although not drilled to date, is inferred to persist at depth (Fig. 8). Zones of quartz plus greenish, illitic clays occur locally within the potassic zone at Filo del Sol but are too restricted to be indicated on cross sections.

Potassic alteration and associated Cu-Au mineralization

Potassic alteration becomes progressively more widespread downward at Filo del Sol and is the main alteration type present in the core of the Aurora zone below an elevation of ~4,200 m (Fig. 8). In contrast, farther south along the Filo del Sol alignment, at Tamberías (Fig. 1b), potassic alteration is exposed at surface at elevations of 5,200 to 5,300 m. The po-

Fig. 6. Field and drill-core images of Filo del Sol area. a. Basal conglomerate of Late Cretaceous volcano-sedimentary sequence unconformably overlying Permian felsic volcanic basement immediately east of Filo del Sol. Conglomerate is largely dominated by pebbles, cobbles, and blocks of underlying volcanic sequence. Hammer for scale. b. Typical, fine-grained to aphanitic microdiorite dike at Filo del Sol. c. Typical amygdaloidal andesite sill at Filo del Sol. Arrows highlight quartz-filled amygdules. d. Intensely veined and altered (K-feldspar, biotite, magnetite) phase 1 porphyry preserved as block within phase 2 porphyry at Filo del Sol. e. Typical phase 2 porphyry at Filo del Sol. Arrow shows large fragment of refractory A-type quartz veinlet. f. Typical phase 3 porphyry at Filo del Sol. Note lack of quartz veinlets and predominance of hornblende and biotite phenocrysts in potassic-stable alteration. g. Monomict, potassic-altered, rhyolite-dominated magmatic-hydrothermal breccia. Note large quartz phenocrysts in rhyolite host and fragments of refractory A-type quartz veinlets indicated by arrows. h. Polymict magmatic-hydrothermal breccia, with fragments of quartz veinlets (shown by arrow), microdiorite, and felsic volcanic rocks. Note throughgoing A-type quartz veinlet, which confirms brecciation during A-veinlet introduction. i. Coarse-grained, pegmatoidal facies of magmatic-hydrothermal breccia, dominated by large K-feldspar aggregates. j. Typical aspect and texture of phreatic breccia emplaced during high-sulfidation mineralization. Abundant equidimensional and irregular fragments of refractory A-type quartz veinlets (shown by arrows) in sulfide- and alunite-bearing, fine-grained lithic matrix showing convolute laminations. k. Close-up view of another phreatic breccia emphasizing equidimensional form of A-type quartz-veinlet fragments (shown by arrows) and granular matrix. l. Close-up view of laminated nature of some phreatic breccia facies (shown by arrows).

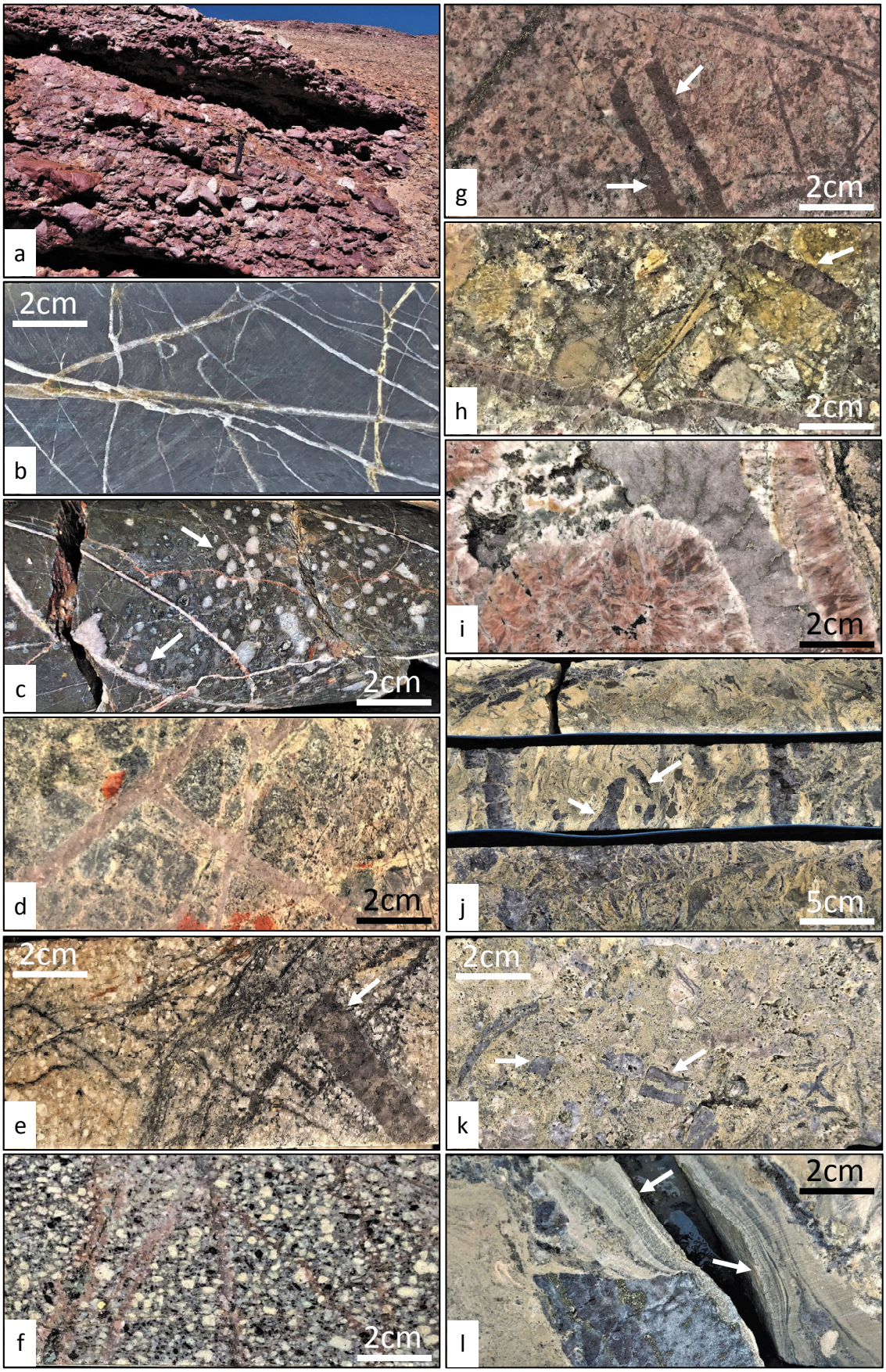

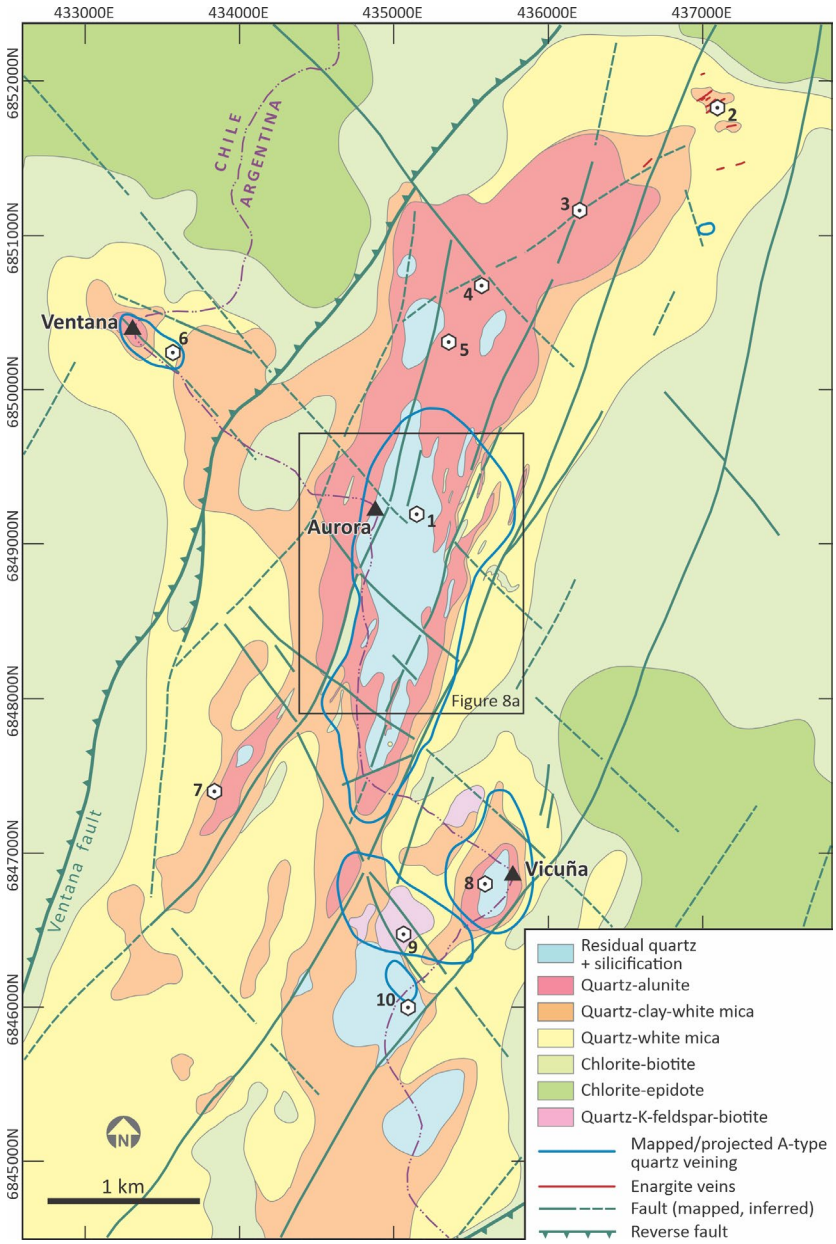

Fig. 7. Surface alteration map of Filo del Sol alignment (see Fig. 4 for reference) highlighting overall dimensions and clear trend of north to northeast advanced argillic lithocap. Clay in the quartz-clay-white mica zone is predominantly kaolinite, with various proportions of dickite. Note outer limit of A-type quartz veining as mapped at surface and/or projected from shallow drill holes. The quartz-veinlet limit follows the north to northeast trend of the Filo del Sol system, but is NW-trending in the Ventana and Tamberías porphyry systems. Also note presence of remnant potassic (quartz-K-feldspar-biotite) alteration at Tamberías and peripheral to Vicuña center, and enargite-bearing veins at Maranceles. The steam-heated overprint is shown in the cross sections of Figure 8. See text for additional descriptions. Prospects and hydrothermal centers are keyed to Figure 4.

tassic alteration in the Aurora zone is characterized by various combinations of quartz, biotite, K-feldspar, magnetite, and anhydrite, and is best developed in early-intermineral porphyry phases and contiguous units, including Triassic monzogranite and the magmatic-hydrothermal breccia. Two main potassic assemblages are recognized: early biotite-magnetite and later quartz-K-feldspar-anhydrite-biotite. An early, hornfels-type assemblage, composed of fine-grained biotite and magnetite with local, probably retrograde chlorite, is present in the andesitic wall rocks and mafic dikes and sills (Fig. 6b, c), whereas the later K-feldspar-bearing assemblage is best developed in the magmatic-hydrothermal breccia, particularly in the pegmatoidal facies (Fig. 9). Biotitic hornfelsed clasts are common in breccia displaying the later potassic assemblage. Hydrothermal magnetite and/or mushketovite (magnetite-replaced specular hematite) are common, comprising ~4 to 5 vol % of the biotitized andesitic country rocks and mafic intrusions and ~2 vol % in porphyry. Iron oxides are also abundant and coarse grained in some facies of hydrothermal breccia (Fig. 9a).

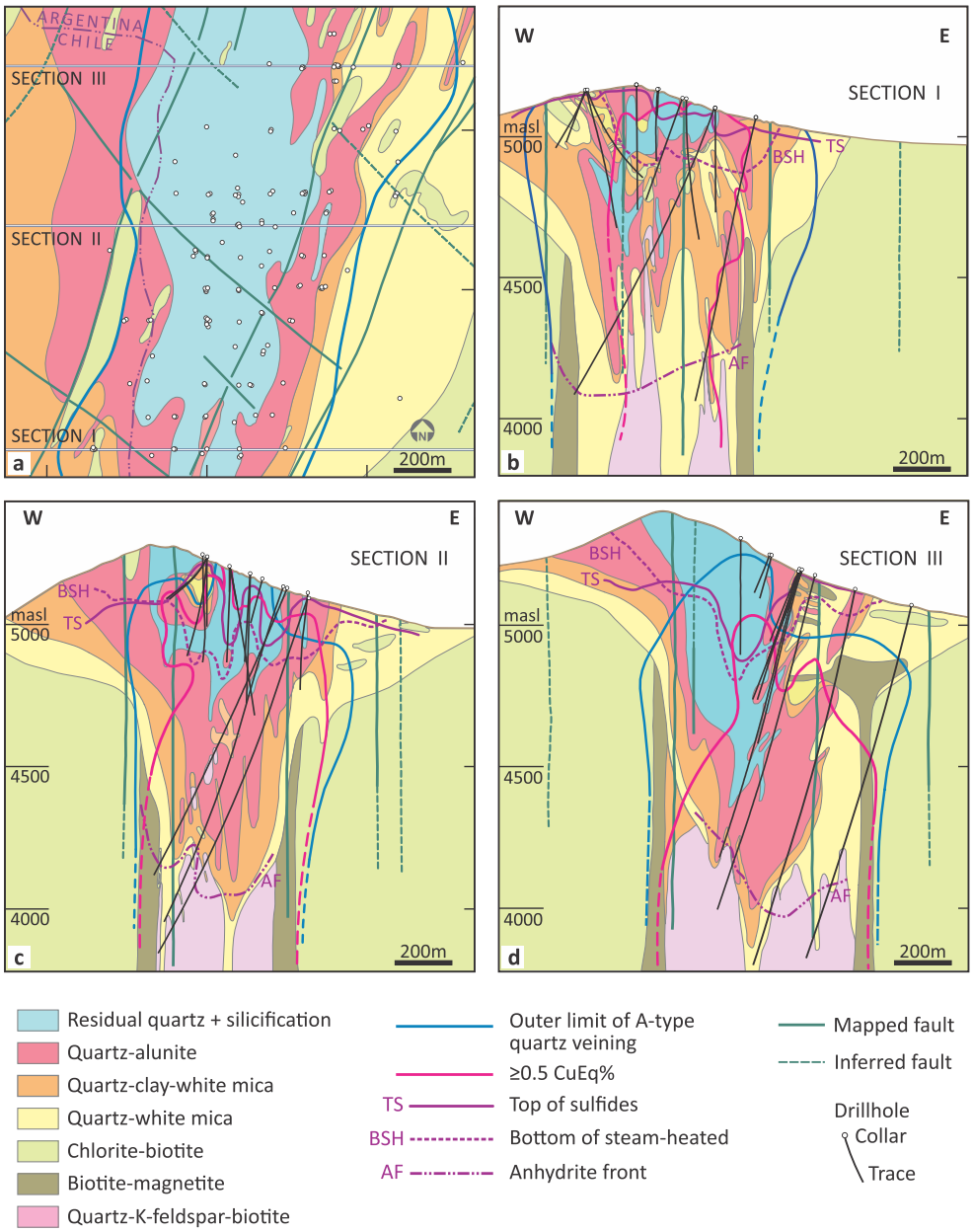

Fig. 8. Alteration associations and zoning at Filo del Sol. a. Plan view to locate cross sections presented as b–d, which are the same as those in Figure 5 b–d. Sections I, II, and III, prepared with a 50-m clipping, showing distribution of principal alteration associations routinely mapped at Filo del Sol. Note porphyry-related potassic alteration partially to entirely overprinted by upward-flared, funnel-shaped advanced argillic zone that forms the most intensely developed part of lithocap. Biotite-magnetite zones are entirely confined to flanking mafic dikes and overlying mafic sills, although in many of the latter biotite was transformed to chlorite and magnetite was martitized. Outer limit of A-type quartz veining, top of sulfides (TS), base of steam-heated alteration (BSH), anhydrite front (AF), and 0.5% CuEq are also marked.

The potassic zone hosts multidirectional, irregular to subplanar veinlets of granular, A-type quartz (Fig. 9b). Hydrothermal magnetite and/or mushketovite are typically present, with magnetite-bearing quartz veinlets generally earlier than those with quartz alone, although the opposite is observed locally. Much of the K-feldspar-bearing potassic assemblage formed during introduction of A-type quartz veinlets, as shown by crosscutting relationships (Fig. 9b, c). Within this late potassic assemblage, biotite formed first and was followed successively by K-feldspar, quartz, anhydrite, and sulfide minerals (Fig. 9c-e). The late potassic alteration is cut by halo-dominant early dark micaceous (EDM)-type veinlets (Meyer, 1965; Proffett, 2009), with or without quartz centerlines, as well as magnetite-bearing early biotite (EB) veinlets that predate the A-type veinlets in deep, internal parts of early-stage porphyry phases (Fig. 9f). EDM-, EB-, and A-type veinlets as well as the K-feldspar-rich assemblage are cut by planar, molybdenite-bearing, B-type quartz veinlets (sensu Gustafson and Hunt, 1975). The EB- and EDM-type veinlets do not constitute coherent, mappable zones, in contrast to A- and B-type veinlets, particu-

larly the former, that occur in all known porphyry and epithermal Cu-Au mineralization at Filo del Sol (Fig. 8).

The sulfides accompanying potassic alteration are chiefly chalcopyrite and pyrite, although minor bornite is present locally with chalcopyrite in pegmatoidal magmatic-hydrothermal breccia. Typically, pyrite is paragenetically earlier than and partially replaced by chalcopyrite in most veinlet types and hydrothermal breccia cements, and where chalcopyrite and bornite occur together, the former is earlier (Fig. 9g, h). Copper and Au contents of 0.4 to 0.6% and 0.3 to 0.5 ppm, respectively, are typical of Filo del Sol potassic alteration, with both metals showing a consistent positive correlation. However, the pegmatoidal breccias can contain much higher grades (>0.8% Cu, >0.6 ppm Au) where coarse-grained chalcopyrite is present (Fig. 9a). Although Au occurs predominantly in its native form (>980 fine), electrum (800 fine) was identified locally. Most of the Au is attached to chalcopyrite, at chalcopyrite-chalcopyrite, chalcopyrite-pyrite, and chalcopyrite-bornite contacts. Some Au occurs as inclusions in Cu sulfides, with a minor proportion free and attached to silicate minerals (G. Di Prisco, unpub. report, 2022). Molybdenum tenors in the potassic zone are ~40 ppm as a result of the partial spatial overlap of molybdenite-bearing A- and B-type veinlets. If Mo was originally concentrated in an annular zone overlapping the outer margin of the Cu-Au center—a characteristic feature of many Au-rich porphyry Cu deposits (e.g., Sillitoe, 1979)—it was masked by the extensive advanced argillic overprint. Silver grades in the potassic assemblages are typical of those in porphyry Cu deposits, averaging 2 to 3 ppm.

The core from a few deep drill holes suggests that the internal parts of the Aurora zone potassic alteration, beneath the main chalcopyrite mineralization, have low total sulfide contents, chiefly pyrite. A-type quartz veinlets in this deep environment at Aurora are either sulfide free or contain few, erratically distributed pyrite grains, further confirming that pyrite was the earliest sulfide.

Advanced argillic alteration and associated high-sulfidation Cu-Au-Ag mineralization

Advanced argillic assemblages, including residual quartz, are by far the predominant alteration types, and their accompanying high sulfidation-state sulfide minerals contain the bulk of the known Cu, Au, and Ag at Filo del Sol, including the highest grades encountered to date in the Aurora zone (Fig. 2d). Four mineral associations are mapped: a central zone of residual quartz, typically with a vuggy texture, that transitions outward to quartz-alunite and quartz-kaolinite to an external quartz-white mica-kaolinite zone (Figs. 7, 8), in common with high-sulfidation Cu-Au-Ag deposits (e.g., Steven and Ratté, 1960) and many porphyry Cu-related lithocaps (Sillitoe, 1995, 2010; Hedenquist and Taran, 2013; Hedenquist and Arribas, 2022). The entire lithocap, ~4.2 km long and averaging ~1.2 km wide, including the 2.3-km-long and 0.8-km-wide Aurora portion, parallels the north to northeast structural trend of the Filo del Sol deposit (Figs. 7, 8a). The upper parts of the lithocap formed at the expense of the Late Cretaceous volcano-sedimentary rocks and, locally, magmatic-hydrothermal and phreatic breccias and late-intermineral porphyry dikes (Figs. 4, 7). At depth, the lithocap is developed in rhyolite-dominated magmatic-hydrothermal breccia and within the main body of early-intermineral porphyry (Figs. 5, 8, 9).

The central part of the advanced argillic lithocap consists of a single large or, more typically, multiple, steeply inclined vuggy residual quartz and silicified bodies with a total north to northeast strike length of at least 2 km (Figs. 7, 8a). Intervening quartz-alunite zones are typical, but where alteration is most intense, as in hole FSDH41 (Fig. 2d), residual quartz predominates. Parallel flanking quartz-alunite alteration contains subsidiary and irregular patches of vuggy residual quartz, with both weakening outward on approach to quartz-clay alteration. The latter has quartz, fine-grained white mica, illite, and kaolinite as principal components, with quartz and white mica becoming predominant at depth and along strike, particularly on the extremities of the system (Fig. 8b). Pyrophyllite, paragonite, and dickite are also present, the first two more common with depth in the quartz-clay zone; the presence of aluminum phosphate-sulfate (APS) minerals is inferred on the basis of elevated P values (2,000–3,800 ppm). The quartz-white mica alteration overprints the early potassic alteration and mineralization, subsequently followed by the residual quartz and quartz-alunite plus clays, which completely or partially destroyed the potassic assemblages (Fig. 8g). Only the flanking mafic dikes (Figs. 5, 8) preserve potassic

Fig. 9. Selected drill-core images depicting porphyry (a–h) and high-sulfidation epithermal (i–n) alteration-mineralization features of Filo del Sol a. Coarse-grained, pegmatoidal mineralization in potassic-altered, K-feldspar-rich, magmatic-hydrothermal breccia. Note large mushketovite crystals indistinctly replaced by chalcopyrite or pyrite. b. Quartz-K-feldspar-biotite-bearing magmatic-hydrothermal breccia. c. Potassic-altered magmatic-hydrothermal breccia with clast of intensely biotitized microdiorite. Note irregular quartz texture and throughgoing A-type quartz veinlet with chalcopyrite and pyrite. d. Pegmatoidal texture in potassic-altered phase 2 porphyry, with K-feldspar, anhydrite, biotite, and chalcopyrite. Note biotite lining to pegmatoidal mass. e. Pegmatoidal texture with biotite, anhydrite, K-feldspar, and quartz. Fine-grained chalcopyrite intergrowths. f. Early dark micaceous (EDM)-type veinlet with fine-grained biotite, K-feldspar, green mica, and chalcopyrite cut by thin A-type quartz veinlets in phase 2, potassic-altered porphyry; both veinlet types are shown by arrows. g. Pegmatoidal quartz-K-feldspar-biotite with end-stage pyrite and chalcopyrite. Where contact relationships are observed, chalcopyrite is paragenetically later than pyrite. h. Close-up view of paragenetic relationship between chalcopyrite and digenite-bornite in A-type quartz veinlet. i. Vuggy residual quartz developed in phase 2 porphyry. Note that A-type quartz veinlets (shown by arrow) remain stable. j. Typical banded high-sulfidation epithermal vein containing alunite, barite, several types of pyrite, and black sulfide minerals. k. High-sulfidation massive sulfide vein containing two principal pyrite generations (1 and 2) described in text plus irregular hairline marcasite veinlet. l. Close-up view of massive sulfide vein with globular and botryoidal marcasite and two principal pyrite generations. m. Close-up view of mesh-type texture (see text) with reticulated, fine-grained pyrite and black, Cu-bearing sulfide minerals. This texture is typical of high-grade, high-sulfidation Cu-Au intervals. n. Close-up view of disseminated, high-sulfidation mineralization, with cores of fine-grained pyrite coated by black, Cu-bearing sulfide minerals. See text for further information. Abbreviations: an = anhydrite, bt = biotite, cpy = chalcopyrite, di-bo = digenite-bornite, ma = marcasite, ms = mushketovite, py = pyrite.

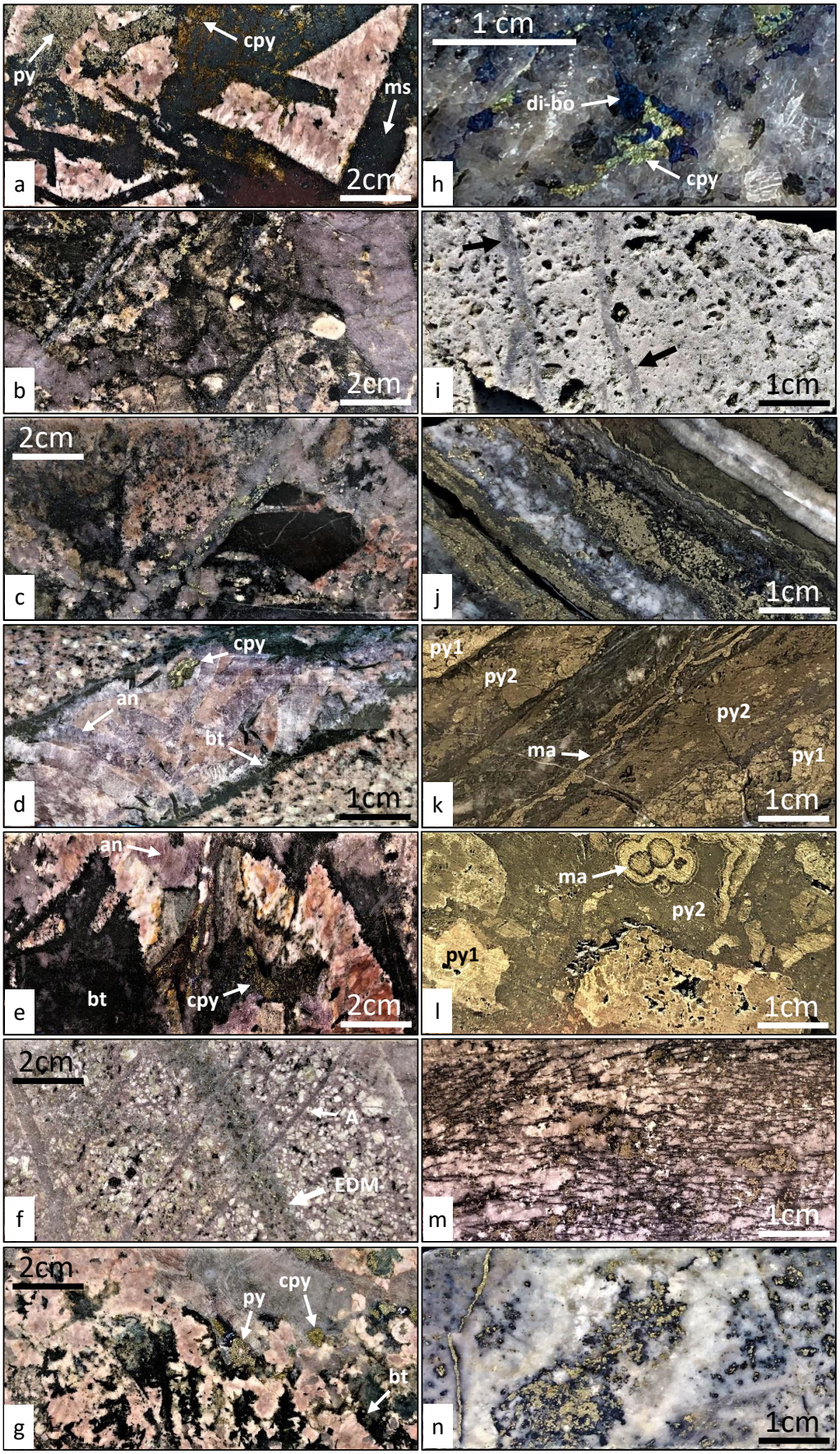

remnants along with pyrite, chalcopyrite, magnetite, and retrograde chlorite. As currently recognized, the advanced argillic alteration defines a steeply dipping, funnel-shaped body that extends to a depth of ~1,000 m, with its topographically highest parts at Aurora preserved along the western side of the porphyry and epithermal deposit (Figs. 7, 8).

The central zone of vuggy residual quartz and silicification as well as the associated quartz-alunite alteration host the Cu-Au-Ag mineralization, including the bonanza-grade zones intercepted by holes FSDH41 and FSDH57 (Fig. 2d). The mineralization comprises multiple, high to very high sulfidation-state sulfide associations with one or more of pyrite, marcasite, and melnikovite-textured pyrite-marcasite, plus Cu sulfides (bornite, digenite, chalcocite, covellite), Cu-As-Sb sulfosalts (enargite, luzonite, famatinite, tennantite), Cu-bearing Ag-As-Sb sulfosalts (pearceite, polybasite), a variety of Ag-bearing sulfides including Ag-As (proustite), Ag-Bi (matildite), and Ag-Sn (canfieldite), as well as numerous although minor occurrences of Ag-Hg-, Ag-Sb-, and Ag-Ge-bearing sulfides, as determined by petrographic work and energy dispersive spectroscopic methods (SEM EDS; G. Di Prisco, unpub. reports, 2018–2022). Native Au, calaverite, electrum, and auricupride (Cu_3Au) are economically and geochemically important components of the high-sulfidation Au mineralization.

At least two high-sulfidation sulfide pulses are represented, pre- and postemplacement of the phreatic breccia body, which contains pyrite-enargite fragments as well as everywhere being affected by high-sulfidation mineralization (Fig. 6j, k). The sulfide minerals occur in a variety of forms, including meter-wide massive sulfide lodes, cements to hydrothermal breccia, veins, veinlets, and disseminations (Fig. 9i–n). A mesh-like texture, comprising reticulated hairline sulfide veinlets, is typical of high-grade zones (Fig. 9m). Pyrite is consistently the earliest sulfide and is progressively replaced by the Cu-As sulfosalts (Fig. 9n) and then chalcocite-group minerals and/or bornite. There are two pyrite generations: early, subhedral, centimeter-scale grains and/or aggregates, and younger, substantially finer-grained, irregular and crenulated, brassy aggregates of subhedral to anhedral, micron-sized grains, occurring as rims around the former (Fig. 9k, l). This second generation is similar to the colloform-textured pyrite bands in the high-sulfidation epithermal mineralization at Agua Rica, Argentina (Franchini et al., 2015), and the brassy phase II pyrite at Pascua, Chile (Chouinard et al., 2005).

Very locally, chalcopyrite occurs as coatings on pyrite; both minerals are overgrown by high sulfidation-state sulfides, implying that minor chalcopyrite formed after development of residual quartz even though it should be metastable under high-sulfidation conditions. In the high-sulfidation mineralization, Cu and Au contents of 0.8 to 0.9% and 0.6 to 0.7 ppm, respectively, are common in zones with >1,000 ppm As and are typically accompanied by Ag values of >25 and ~70 ppm Mo, implying that the high sulfidation-state sulfides involved important metal addition. As well as Cu, Au, Ag, and Mo, the high-sulfidation mineralization in the Aurora zone contains much higher As, Sb, Bi, Co, Cr, Hg, Ni, Pb, S, Sn, Re, W, and Te values than the preexisting potassic associations, whereas Ba, Ca, Mg, Mn, Na, Ti, U, V, and Zn tend to be lower. Limited electron microprobe analyses (EMA) show that pyrite of the high-sulfidation stage hosts variable concentrations of As (400–2,800 ppm), Cu (100–26,000 ppm), Co (500–900 ppm), Ag (0–2,300 ppm), and Bi (100–1,200 ppm); the dominant, early pyrite generation averages 500 ppm As and the younger, brassy pyrite contains as much as 2,800 ppm As (G. Di Prisco, unpub. report, 2022).

Steam-heated alteration

The steam-heated zone at Aurora is prominently developed for ~1 km along the ridge between Argentina and Chile. The blanket-like zone, interpreted to have developed above a paleogroundwater table, occupies the shallow parts of the system where it is exposed at elevations of ~5,100–5,400 m and attains a thickness of ~200 m beneath the ridge crest (Fig. 8b-d). Downward-penetrating roots extend for up to ~400 m deeper, controlled by vertical faults, their damage zones, and lithologic units, such as phreatic breccia, mafic dike contacts, and previously formed vuggy residual quartz. The steam-heated zone is composed of white, powdery, low-density rock containing opal CT, chalcedony, kaolinite, and alunite, with local native S and cinnabar, in common with steam-heated alteration elsewhere (e.g., Sillitoe, 1993; Hedenquist and Arribas, 2022). The steam-heated zone is characteristically barren of metals, except for where there are local remnants of preexisting high-sulfidation Cu, Au, and Ag mineralization or their supergene products.

Structure

As described above, the regional structure of the Vicuña belt (Fig. 3) is characterized by a series of N- to NE-trending, steep to moderate, E- or W-dipping reverse faults that control the distribution of similar trending blocks of basement granitoids and felsic volcanic rocks (e.g., Martínez et al., 2015b, 2016, 2018). Two principal faults, El Potro in Chile and the Mogotes zone in Argentina, appear to constitute the bounding structures of a large, pop-up, basement-cored block cut internally by subsidiary reverse faults (e.g., Ventana and Los Helados faults), which served as loci for the Filo del Sol alignment (Fig. 3). The basement blocks are inferred to be shallow expressions of E-propagated, thick-skinned ramps that accommodated the regional shortening (e.g., Martínez et al., 2015b, 2016). Numerous NW-trending lineaments are apparent on satellite imagery and geophysical magnetic surveys, but only a few can be mapped or inferred as faults in the field (Fig. 3a; Devine et al., 2019; Sillitoe et al., 2019). Some of them likely formed as conjugate structures to the reverse faults.

Two principal families of faults, pre- and postmineral in timing, are present in the Filo del Sol area, and many of the premineral structures are inferred to have influenced the magmatic-hydrothermal system (Figs. 4, 5). The dominant north to northeast trend of the system is congruent with the regional structural grain described above and constitutes a first-order control for Filo del Sol and the Filo del Sol alignment (Fig. 1b). The main premineral structure was inherited from the basement where it controlled the contact between the monzogranite pluton, mostly located to the west, and the felsic volcanic sequence farther east (Figs. 3b, 4, 5). This important steep contact was likely subhorizontal during granitoid intrusion, as suggested by the abundant aplite bodies originally defining its cupola, before undergoing inversion as a west-

over-east reverse fault, with preservation of the felsic volcanic sequence on its eastern footwall side. Where observed in drill core, the structure is characterized by mylonitic fabric, intruded by undeformed mafic dikes. The similar W-dipping Ventana reverse fault, west of Filo del Sol, controls the position of a parallel granitoid block, and the similarly oriented, albeit E-dipping Los Helados reverse fault is spatially related to several porphyry deposits and prospects, including Los Helados (Fig. 3a). Emplacement of the Josemaría deposit, located on a similar, but separate basement block to the east (Fig. 3a), is also inferred to have been originally controlled by a high-angle fault, with east-over-west reverse movement during the late Oligocene (25–24 Ma; Sillitoe et al., 2019). These and other E- and W-dipping reverse faults mapped in the Vicuña belt and surroundings were inverted from original normal faults that controlled sites of marine and continental basin construction and sedimentation during successive Mesozoic and Cenozoic extensional events (Martínez et al., 2015a, b, 2016, 2018; Sillitoe et al., 2019).

Conjugate, NW-trending faults are also inferred to have been active at the same time and provided magmatic-hydrothermal conduits for porphyry Cu formation. The most obvious examples of consequent porphyry development are the NW-trending porphyry intrusion and associated Cu-Au-bearing quartz-veinlet stockworks at Tamberías and the northwest trend defined by the Ventana and Vicuña porphyry stocks and their contained sheeted quartz-veinlet arrays (Figs. 1b, 4, 7).

A series of steep, N- to NE-striking, postmineral faults transect the Filo del Sol alignment and display recent activity, indicated by solifluction and illustrated by topographic breaks and drainage offsets, as well as by meter-scale zones of intensely fractured rock in drill core from the Filo del Sol deposit (Figs. 4, 5). These recent fault displacements do not exceed a few meters. Most of these reactivated faults are considered to have minor strike-slip and down-to-the-east normal displacements, although both east- and west-side-down offsets are apparent in surface exposures. Postmineral movement along the NW-trending faults has also been mapped and/or inferred locally (Fig. 4).

Silver Mineralization Zone

The Filo del Sol deposit is characterized by a 20- to 80-m-thick zone of elevated (>60 ppm) Ag values that extends north for 1,600 m to the Aurora zone. To the north of the Aurora zone, limited drilling shows that >60-ppm Ag mineralization may extend for an additional 400 m. The Ag-rich zone is confined to a central, 200- to 400-m-wide corridor of high-sulfidation lodes and deepens progressively to the north beneath the steam-heated horizon and remnants of residual quartz and quartz-alunite alteration (e.g., Devine et al, 2019). Detailed cross-section construction shows no evidence for deposit-wide lithologic or stratigraphic control.

The Ag-rich zone is typified by unconsolidated, gray to black muddy material, in which Ag is present as chlorargyrite, acanthite, and native Ag plus numerous Ag-As-Sb-bearing sulfosalts, chiefly proustite and pyrargyrite (G. Di Prisco, unpub. report, 2019). Nevertheless, local kilogram-grade Ag intercepts lack macroscopically observable Ag minerals. The Ag-rich intervals contain a variety of metal associations independent of the host rock and position of the zone relative to the base of supergene oxidation, although high-grade (>100 ppm), muddy material generally occurs in the general vicinity of the redox front. For example, phreatic breccia is an important, but not exclusive, host to the high-grade Ag; faults and associated damage zones, as well as high-sulfidation lodes, can also control Ag distribution and concentration. In general, the Ag zone has a distinct geochemical signature, with anomalous values of one or more of Cu, Ag, Mo, Sb, Au, As, Hg, W, Bi, and Sn, essentially identical to the geochemical fingerprint of the high-sulfidation mineralization elsewhere at the Aurora zone and Filo del Sol deposit.

Supergene Effects

An anomalously thick, albeit irregular zone of supergene sulfide oxidation is present in the Filo del Sol area, including the Aurora zone, where it reaches a maximum thickness of ~300 m below the ridge crest but is much thinner below the ridge flanks (Fig. 8b-d). The oxidized zone comprises three subzones: upper leached, intermediate oxidized, and lower mixed oxide-sulfide, followed at depth by localized Cu sulfide enrichment. The upper leached zone is mainly developed at the expense of former steam-heated alteration and vuggy residual quartz, in which all pyrite and other sulfide minerals, and including essentially all contained Cu, have been completely oxidized and removed, although some Au remains (Devine et al., 2019). Indeed, native Au is the most common mineral reported from the leached zone, where it is encapsulated in quartz and/or Fe-bearing sulfates, mainly jarosite. Copiapite, coquimbite, römerite, and halotrichite are common, and cuprocopiapite is responsible for local anomalous Cu values (Fig. 10). Chenevixite and scorodite are also observed in places, likely derived from oxidative destruction of enargite. The intermediate oxidized zone contains Fe, Fe-Cu, Cu, Mo, and Co oxides and hydroxides and hosts most of the soluble Cu mineralization in the Filo del Sol open-pittable resource (see above; Devine et al., 2019). This resource is dominated by water-soluble chalcanthite along with subordinate antlerite, brochantite, cyanotrichite ($Cu_4\ Al_2\ [(OH_{12}SO_4]\cdot 2H_2O$), and cuprocopiapite (Fig. 10). Ilsemannite is also characteristic of this zone and erythrite, probably derived from cobaltian pyrite, is locally present (Fig. 10g, h). Residual enargite is present suprajacent to the lower mixed zone, and sooty chalcocite defines local pockets of supergene sulfide enrichment. As a result of the steep, glaciated topography, most of the Cu leached from the oxidized zone appears to have been dissipated in either the vadose zone or surface streams rather than having descended to enrich hypogene sulfide minerals beneath the groundwater table.

Anhydrite front

Both the porphyry and epithermal mineralization styles at Filo del Sol contain variable amounts of anhydrite, much of it in the former. In the deep parts of the system, where potassic alteration is preserved, anhydrite is a common component of the early-stage, magmatic-hydrothermal breccia and crosscutting A-type veinlets. One breccia variety includes anhydrite masses up to several tens of meters wide, in which it is intergrown with pegmatoidal biotite and/or K-feldspar (see above). In the high-sulfidation overprint, anhydrite is part of sulfide-bearing lodes, hydrothermal breccias, and veins, the last with

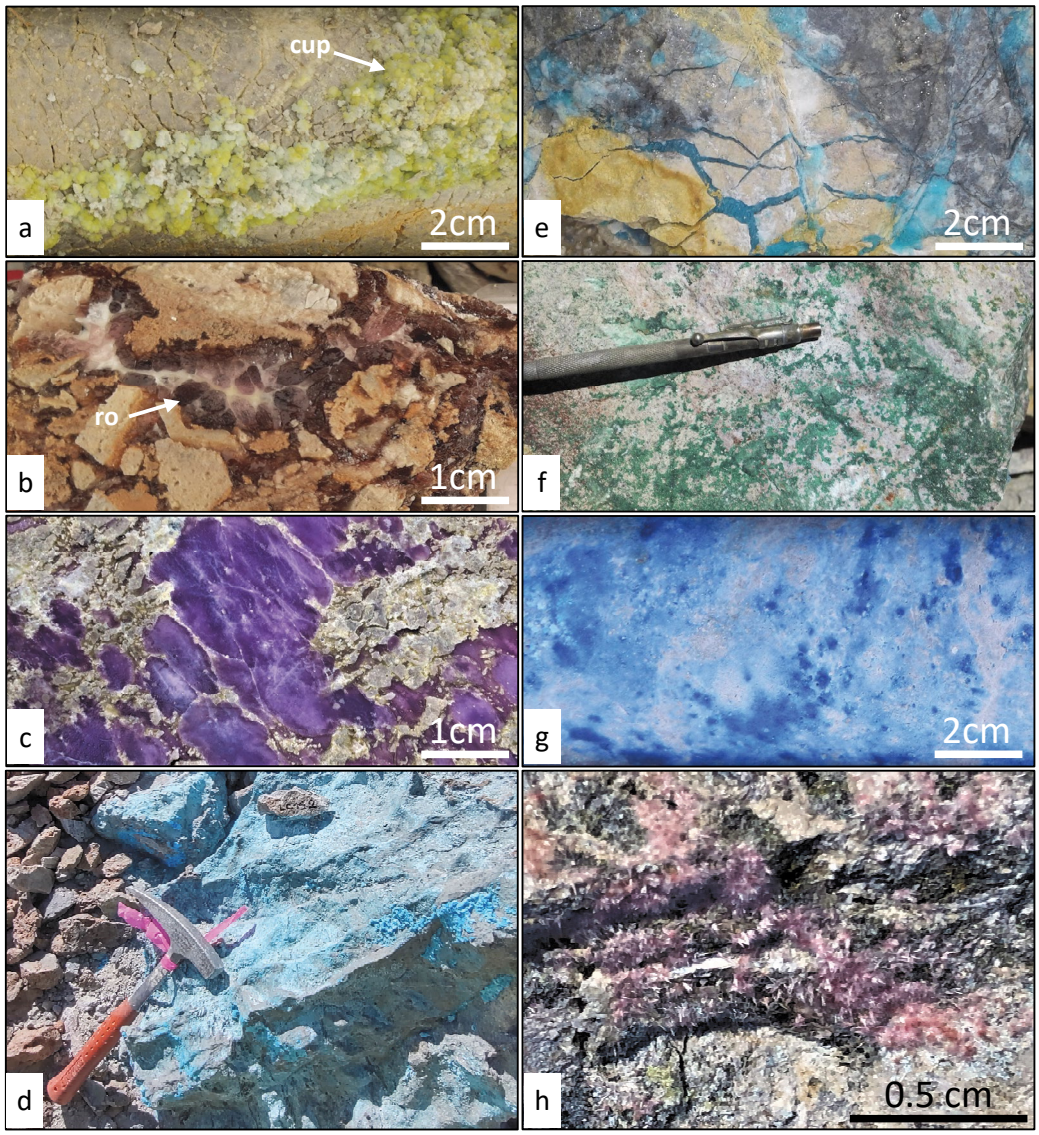

Fig. 10. Field and drill-core images showing supergene products at Filo del Sol. a. Typical occurrence of yellowish cuprocopiapite. b. Fracture filled by vitreous brown römerite. c. Massive purplish violet coquimbite. d. Close-up view of chalcanthite (see Fig. 1c for location). Hammer for scale. e. Chalcanthite-filled fractures in drill core. f. Close-up view of brochantite from outcrop. Scribe for scale. g. Fine-grained disseminations of light- to deep-blue ilsemannite. h. Close-up view of delicate crystal growths of pale-rose and pinkish erythrite. Abbreviations: cup = cuprocopiapite, ro = römerite.

local barite. The former presence of anhydrite is indicated by characteristic open spaces present in veinlets and breccias, from which it was dissolved by cool meteoric groundwater. The transition of anhydrite to gypsum, preparatory to dissolution of the latter, is observed over intervals of a few to ~200 m, with the resultant top-of-anhydrite front currently at an average depth of ~1,100 m below surface in the central parts of the deposit, but much shallower on its margins (Fig. 8b–d).

Geochronology

U-Pb zircon ages of country rocks

Six U-Pb dates (Table 1; App. 1) for samples from the basement felsic volcanic sequence, collected from surface and drill holes at Filo del Sol and surroundings, range in age from 268.7 ± 2.6 to 250.6 ± 1.5 Ma (middle Permian to earliest Triassic), whereas one sample (FSDH034C-1038; Table 1; App. 1) from the crosscutting monzogranite returned an age of 231.8 ± 3.2 Ma (Middle Triassic; 93.5% confidence from coherent group of 11 points). Two rhyolite samples contain one zircon each of Paleoproterozoic (2394 Ma) and Mesoproterozoic (1591 Ma) ages (samples FSDATA05 and FSDATA08, respectively; App. 1), possibly incorporated from underlying Devonian–Carboniferous siliciclastic sequences that are exposed a few kilometers southwest of Filo del Sol in Chile (e.g., Palape et al., 2015; Salazar and Coloma, 2016). Detrital zircons of Precambrian age from these siliciclastic rocks are interpreted to have a distal eastern provenance from the Brazilian Shield (Palape et al., 2015; Salazar and Coloma, 2016). The ages obtained from the felsic sequence confirm its formation during the regional Choiyoi event (see above), whereas the age of the monzogranite shows it to be part of the Chollay batholith

exposed on the Chilean side of the border, where it is dated at 246 to 235 Ma (Martínez et al., 2015a, b; Salazar and Coloma, 2016). The nearest batholithic exposures in Chile, ~2 km west of the Filo del Sol area (Fig. 3a), have been assigned to either the Chollay granite (Martínez et al., 2015b) or an older granitoid unit, the Montosa-El Potro batholith with an age of 265 to 245 Ma (Martínez et al., 2015a). A large population of zircon grains with ages between 260 and 240 Ma from the Aurora monzogranite were likely inherited from the Montosa-El Potro batholith (sample FSDH034C-1038; App. 1).

The age of the volcano-sedimentary sequence is constrained by two samples from roadcuts at the Vicuña prospect. Sample FSDATA12 (Table 1) has a maximum depositional age of 75.2 ± 0.9 Ma, representing a 95% confidence of a coherent group of eight detrital zircons, in addition to containing 72 detrital zircons derived from basement rocks with ages between 300 and 250 Ma (App. 1). A second sample (FSDATA24), from a fine-grained, laminated volcaniclastic horizon of andesitic composition higher in the sequence, returned an age of 67.5 ± 0.4 Ma, representing a 95% confidence of a coherent group of 34 points; both dates confirm the Late Cretaceous timing of the sequence. These samples, as well as others not reported herein, contain detrital zircon populations of 99–80, 160–102, and 300–250 Ma, suggesting measurable contributions from not only nearby basement granitoids, but also sequences now preserved west of the border in Chile (e.g., Martínez et al., 2015a; Salazar and Coloma, 2016).

Multiple mafic dike phases are confirmed by three dated samples from the Filo del Sol alignment. Sample FSDATA16, from the southern part of the alignment, yielded a 37.0 ± 1.3-Ma age, representing a 95% confidence of a coherent group of four points (Table 1; App. 1), whereas sample FSDH21-10 from the Filo del Sol deposit yielded an age of 81.9 ± 0.7 Ma, representing a 95% confidence from a coherent group of three points (Table 1; App. 1). Interestingly, both samples contain inherited zircons from older rocks, with population peaks at 266, 254, 233, and 123 Ma (App. 1). These two ages confirm established geologic relationships and show that many of the mafic dikes are premineral, although the 15.8 + 0.2/–0.3-Ma age yielded by sample FSDH54-24 (95% confidence from a coherent group of 34 points; Table 1; App. 1) implies that some mafic phases were precursors to, or broadly contemporaneous with, porphyry Cu intrusions in the Aurora zone and elsewhere along the Filo del Sol alignment. Sample FSDH54-24 also contains a second zircon population dated at 35 to 34 Ma, identical to the porphyry Cu-Au prospect at Flamenco (Fig. 1b) and other deposits and prospects in the region (Perelló et al., 1996; Martínez et al., 2015a).

U-Pb zircon ages of Filo del Sol porphyry phases

The six U-Pb ages reported herein for Filo del Sol (Table 1) include one by the ID-TIMS method (sample 15FD872; F. Devine and R. Friedman, unpub. report, 2015; Devine et al., 2019) and five by the LA-ICP-MS method (samples FSDH25-773, FSDH32A-752, FSDH43-396, FSDH46-1093, FSDH46-1452). All samples returned geologically constrained ages for the early- and late-intermineral porphyry phases, which reveal overlapping emplacement histories between 15.6 and 15.0 Ma (Langhian, middle Miocene; Table 1; App. 1). Three samples from early-intermineral phases at Filo del Sol yielded ages of 15.6 + 0.4/–0.3 (sample FSDH046-1093; 94.3% confidence from coherent group of 14 points), 15.2 ± 0.5 (sample FSDH025-773; 96.9% confidence from a coherent group of 6 points), and 15.0 + 0.3/–0.4 Ma (sample FSDH32A-752; 97.9% confidence from coherent group of 16 points), whereas two late-intermineral phases, one exposed in the Aurora zone (sample 15FD872) and another (sample FSDH046-1452) from a deep-seated dike, returned an ID-TIMS age of 15.475 ± 0.042 Ma and a MS-ICP-LA age of 15.2 + 0.3/–0.2 Ma (97.7% confidence from coherent group of 24 points), respectively. Additionally, sample FSDH43-396 (Table 1; App. 1), from an intermineral dike at the Refugio center, ~400 m northeast of the Aurora zone along the Filo del Sol alignment, yielded an age of 15.6 ± 0.4 Ma (93.5% confidence from a coherent group of 11 points). Importantly, the three youngest zircon ages from all samples of these porphyry phases range from 15.0 to 14.0 Ma, with dominant populations from 14.5 to 14.3 Ma (App. 1), which could be taken to approximate emplacement ages (cf. Buret et al., 2016; Large et al., 2020). Furthermore, the magma that formed most of these intrusions inherited zircons with ages of 37 to 33 Ma, likely reflecting the magmatic-hydrothermal event that generated the porphyry Cu-Au prospect at Flamenco and other deposits nearby in Chile (e.g., La Fortuna; Perelló et al., 1996).

Re-Os molybdenite ages of mineralization

Re-Os dates for porphyry and epithermal molybdenite samples document multiple mineralization pulses along the Filo del Sol alignment, with model ages from 15.1 to 14.1 Ma, and all but one of the 17 from the Aurora zone ranging from 14.75 to 14.41 Ma (Table 2). At the Aurora zone, the oldest date, 15.08 ± 0.06 Ma, is for molybdenite from an A-type quartz veinlet that was subsequently reopened and filled by pyrite and enargite (sample FSDH62-676). In contrast, molybdenite from a granular, A-type quartz veinlet with chalcopyrite and bornite cutting potassic-altered phase 2 porphyry yielded a younger age, 14.58 ± 0.06 Ma (sample FSDH67-1172) and a molybdenite-only veinlet with a conspicuous K-feldspar alteration halo, also cutting phase 2 porphyry, returned an identical age of 14.60 ± 0.06 Ma (sample FSDH67-1043). Similarly, two other K-feldspar- and chalcopyrite-bearing A-type veinlets in phase 2 porphyry yielded ages of 14.62 ± 0.06 (sample FSDH67-1028) and 14.57 ± 0.06 Ma (sample FSDH58-1034).

Molybdenite from typical porphyry-related, B-type quartz veinlets in both shallow and deep parts of the Aurora zone returned ages of 14.75 ± 0.06 (sample FSDH06-322.5), 14.56 ± 0.06 (sample FSDH71-357), 14.63 ± 0.06 (sample FSDH64-1322), and 14.45 ± 0.06 Ma (sample FSDH54-1107), whereas a B-type quartz-veinlet fragment in phreatic breccia yielded an age of 14.59 ± 0.06 Ma (sample FSDH57-415). Molybdenite from a scarce D-type veinlet gave an age of 14.41 ± 0.06 Ma (FSDH32A-951), slightly younger (~0.1 m.y.) than all but one sample from the B-veinlets; six different molybdenite samples from the high-sulfidation epithermal overprint, all intimately associated with quartz-alunite alteration, yielded a similar range of ages to the B-type quartz veinlets of 14.74 ± 0.06 (sample FSDH21-152), 14.64 ± 0.07 (sample FSDH64-901), 14.58 ± 0.06 (sample FSDH70A-588), 14.45 ± 0.06 (samples FSDH61-553.9 and FSDH69A-659), and 14.44

Table 2. Re-Os Isotope and Age Data for Molybdenite, Filo del Sol Alignment and Aurora Zone

Sample	UTM[1] N/E	Re ppm	±2σ	^{187}Re ppm	±2σ	^{187}Os ppb	±2σ	Model age (Ma)	±2σ	Comments
FSDH62-676	6848899/435597	262.5	0.7	165.0	0.5	41.457	0.004	15.08	0.06	A-type veinlet, Aurora zone
FSDH67-1028	6848800/435298	363.4	1.0	228.4	0.6	55.639	0.008	14.62	0.06	A-type veinlet, Aurora zone
FSDH67-1043	6848800/435298	1175	3	738.5	2.1	179.643	0.017	14.60	0.06	A-type veinlet, Aurora zone
FSDH67-1172	6848800/435298	237.4	0.7	149.2	0.4	36.2605	0.008	14.58	0.06	A-type veinlet, Aurora zone
FSDH58-1034	6848741/435374	62.71	0.18	39.42	0.11	9.5709	0.0037	14.57	0.06	A-type veinlet, Aurora zone
FSDH06-322.5	6847800/434900	1360	4	854.6	2.5	210.1	0.2	14.75	0.06	B-type veinlet, Aurora zone
FSDH54-1107	6849192/435455	89.82	0.25	56.454	0.158	13.59	0.02	14.45	0.06	B-type veinlet, Aurora zone
FSDH57-415	6849398/435406	123.0	0.3	77.29	0.22	18.784	0.022	14.59	0.06	B-type veinlet fragment in breccia, Aurora zone
FSDH71-357	6849403/435620	233.7	0.7	146.9	0.4	35.632	0.010	14.56	0.06	B-type veinlet, Aurora zone
FSDH64-1322	6848799/435197	360.5	1.0	226.6	0.6	55.255	0.033	14.63	0.06	B-type veinlet, Aurora zone
FSDH32A-951	6849002/435416	811.9	2.3	510.3	1.4	122.5	0.1	14.41	0.06	D-type veinlet, Filo del Sol
FSDH21-152	6848100/434993	610.3	1.8	383.6	1.1	94.19	0.08	14.74	0.06	High-sulfidation, Filo del Sol
FSDH64-901[2]	6848799/435197	49.27	0.14	30.97	0.09	7.5525	0.0139	14.64	0.07	High-sulfidation, Aurora zone
FSDH69A-659	6849391/435405	395.5	1.1	248.6	0.7	59.844	0.004	14.45	0.06	High sulfidation, Aurora zone
FSDH61-553.9	6849505/435598	422.2	1.2	265.3	0.7	63.891	0.007	14.45	0.06	High-sulfidation, Aurora zone
FSDH54-1043[2]	6849192/435455	10.17	0.03	6.394	0.018	1.538	0.003	14.44	0.07	High-sulfidation, Aurora zone
FSDH70A-588	6849012/435505	99.76	0.28	62.71	0.18	15.234	0.005	14.58	0.06	High-sulfidation, Aurora zone
FSDH43-326	6850160/435427	55.82	0.16	35.088	0.098	8.463	0.007	14.48	0.06	B-type veinlet, Refugio center
FSDH43-816[2]	6850160/435427	0.7507	0.0021	0.4719	0.0013	0.1134	0.0009	14.42	0.13	High-sulfidation, Refugio center
FSDH60-1067.5	6851048/436073	280.3	0.8	176.2	0.5	42.052	0.009	14.33	0.06	A-type veinlet, La Bonita
FSDH60-783.7	6851048/436073	655.6	1.8	412.1	1.2	97.098	0.018	14.14	0.06	High-sulfidation, La Bonita center
FSDATA27	6850796/435463	24.88	0.07	15.64	0.04	69.464	0.007	266.1	1.1	Quartz-molybdenite veinlet, El Viejo center

Notes: See Appendix 2 for methods and other analytical data; ppb = parts per billion; ppm = parts per million; all uncertainties are quoted at the 2σ level of precision

[1] UTM projection WGS84-zone 19

[2] Mineral separate contains silicate impurities which do not affect the Re-Os age, but dilute the Re and Os abundances

± 0.07 Ma (sample FSDH54-1043), the last two overlapping with the age of the D-type veinlet. The molybdenite from sample FSDH64-901 is associated with disseminated pyrite and contained in the fine-grained, laminated matrix of a phreatic breccia dike, whereas molybdenite in sample FSDH54-1043 is from a massive, high-sulfidation sulfide vein in which pyrite is coated by intergrown enargite and molybdenite. In combination, the isotopic age data confirm that the porphyry and high-sulfidation epithermal mineralization at Filo del Sol, and the Aurora zone in particular, took place over a short period, mostly (90% of samples) within ~0.35 (± ~0.06) m.y. in the middle Miocene (Langhian), consistent with the U-Pb zircon dates for the porphyry intrusions, particularly if their youngest 14.5- to 14.3-Ma zircon populations are considered to denote final emplacement ages.

Four additional Re-Os dates for molybdenite from the Refugio and La Bonita centers (Table 2) further confirm the same timing for sulfide mineralization along the entire Filo del Sol alignment. At Refugio, molybdenite from a porphyry-related B-type quartz veinlet returned an age of 14.48 ± 0.06 Ma (sample FSDH43-326), and molybdenite predating pyrite and enargite in an alunite-bearing, high-sulfidation vein yielded an age of 14.42 ± 0.13 Ma (sample FSDH43-816). Similarly, at La Bonita, molybdenite from a chalcopyrite-bearing, A-type quartz veinlet deep in the system gave an age of 14.33 ± 0.06 Ma (sample FSDH60-1067.5), whereas molybdenite

from a high-sulfidation pyrite-enargite-covellite assemblage yielded an age of 14.14 ± 0.06 Ma (sample FSDH60-783.7).

Interestingly, a coarse rosette of molybdenite accompanying pyrite from the centerline of a centimeter-wide quartz veinlet in the El Viejo area (Figs. 1b, 4; sample FSDATA27; Table 2) returned a model age of 266 ± 1.1 Ma, consistent with those for the host middle Permian felsic volcanic and subvolcanic basement rocks. The ~1 km² El Viejo area is characterized by quartz-veinlet stockworks in rhyolite porphyry that report anomalous Mo (100–140 ppm) and Bi (up to 110 ppm) values in grid-sampled talus-fines, perhaps indicative of a porphyry Mo system (J. Perelló, unpub. report, 2022).

K-Ar alunite ages for alteration

Two samples of fine-grained, white, powdery alunite from the steam-heated zone at Aurora, one from surface (17FD030) and the other from its deeper parts (FSDH023-230), are interpreted to be of steam-heated origin on the basis of texture and association; they yielded ages of 12.0 ± 2.4 and 12.7 ± 0.9 Ma, respectively (Table 3). Coarse-grained, crystalline alunite present as patches in a zone of intense quartz-alunite alteration (sample FSDH011-150) returned an age of 13.9 ± 1.6 Ma (Table 3), which is interpreted to represent the timing of the quartz-alunite facies of the hypogene overprint at Filo del Sol, broadly coincident with the higher resolution Re-Os molybdenite dates.

Discussion

Exploration and discovery

Although the Cu mineralization indicated by the spectacular chalcanthite showings at Filo del Sol (Fig. 1c) was observed by initial explorers nearly 25 years ago, and the existence of porphyry-type mineralization was quickly identified during the ensuing exploration, formal discovery and resource definition of the Filo del Sol deposit took ~17 more years. Exploration success by the Lundin Group at higher priority targets in the region slowed work in the Filo del Sol area and the discovery of the Aurora zone. Promulgation of a mining treaty between Chile and Argentina facilitated cross-border exploration activities. Geologic mapping and geochemistry along with timely reassessment of historical geophysical and SWIR surveys led to improved understanding of the district- and local-scale geologic framework. The first deep core hole sited using the revised geologic criteria encountered a potassic-altered, porphyry Cu-bearing intrusion, confirming long-standing geologic predictions. Definition of N-pointing vectors underpinned siting of the discovery hole in the high-grade Aurora mineralization. Advances in drilling technology, as well as the expertise gained by drillers over years of work in the area, were critical when drilling deep holes (up to ~1,800 m) collared in friable steam-heated alteration at high altitude (>5,000 m). Long-term management support for the project, notwithstanding difficult topographic, climatic, access, and drilling conditions, was fundamental to discovery.

Porphyry Cu-Au mineralization

The porphyry Cu-Au mineralization at Filo del Sol shares the main attributes of many Au-rich porphyry Cu deposits worldwide, including elevated hydrothermal magnetite contents in potassic alteration and a reasonable correlation between Cu and Au tenors (cf. Sillitoe, 1979, 2000). The presence of mushketovite is, however, unusual, although reported from porphyry Cu deposits elsewhere (e.g., Río Blanco-Los Bronces, central Chile; Frikken et al., 2005). The positive Cu-Au correlation is confirmed by the intimate association of native Au and Cu-bearing sulfides, predominantly chalcopyrite, probably as a result of coprecipitation given the relatively shallow emplacement depth (cf. Murakami et al., 2010).

Of the three main porphyry phases currently recognized at Filo del Sol, the early-intermineral phase 2 porphyry is associated with most of the porphyry Cu-Au mineralization introduced during potassic alteration (Figs. 5, 11). Phase 1 porphyry is preserved only locally as blocks and clasts in early-stage magmatic-hydrothermal breccia and phase 2 porphyry. The late-intermineral phase 3 porphyry truncates earlier-formed quartz veinlets and sulfides as well as hosting low-grade Cu-Au mineralization. The main porphyry Cu-Au mineralization is centered on the N- to NE-trending porphyry corridor, defined by the three spatially coincident porphyry phases and associated magmatic-hydrothermal breccia, the latter largely dominated by felsic volcanic clasts. The premineral mafic intrusions flanking and overlying the porphyry dikes are inferred to have exerted a measure of spatial-physical control on deposit localization (Fig. 5).

A notable feature of the porphyry Cu-Au mineralization at Filo del Sol is the dominance of early A-type quartz veinlets (e.g., Fig. 8). B-type veinlets contribute Mo in addition to Cu and Au, but are far more restricted in both number and extent. The mineralized A-type veinlet stockworks are spatially and temporally associated with the upper and intermediate parts of early-intermineral porphyry phases 1 and 2 (Figs. 5, 8). The early-stage magmatic-hydrothermal breccia is an important host for Cu-Au mineralization, particularly where it is pegmatoidal and has coarse-grained chalcopyrite in the cement (Figs. 9, 11). To drilled depths, bornite is not a significant contributor to Cu grade, and obvious bornite-dominated zones are absent. Chalcopyrite is rarely observed as the sole sulfide, although there are zones with high chalcopyrite/pyrite ratios in pristine potassic alteration. Irrespective of whether

Table 3. K-Ar Age Data for Alunite, Filo del Sol Deposit

Sample	UTM[1] N/E	%K	Radiogenic Ar (Nl/g)	% Atmospheric Ar	Age, Ma ± 2σ	Comments
17FD030	6848723/ 435320	0.836	0.3901	88.2	12.0 ± 2.4	Steam-heated
FSDH23-230	6848103/ 434995	1.057	0.5224	79.9	12.7 ± 0.9	Steam-heated
FSDH011-150	6848400/ 435000	4.203	2.2788	84.4	13.9 ± 1.6	Advanced argillic alteration

Analyses and dating by Servicio Nacional de Geología y Minería (SERNAGEOMIN), Santiago, Chile
[1]UTM projection WGS84-zone 19

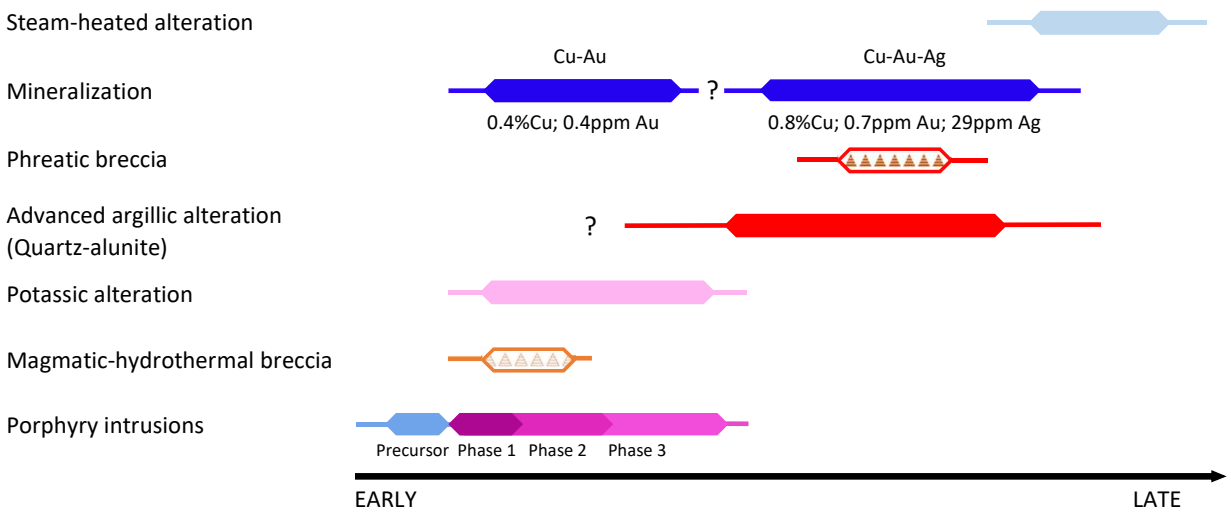

Fig. 11. Schematic timeline diagram showing relative age relationships between main porphyry Cu-Au and high-sulfidation epithermal Cu-Au-Ag mineralization events at Filo del Sol and associated porphyry intrusion, brecciation, and hydrothermal alteration. Note increased Cu tenors corresponding to high-sulfidation event, indicating hypogene metal enrichment.

or not chalcopyrite is the dominant sulfide, the paragenetic sequence commenced with pyrite, which was later partially or wholly transformed to chalcopyrite, thereby defining a system-wide Fe to Cu temporal trend (cf. Far Southeast, Philippines; Calder et al., 2022).

Although still poorly defined by drilling, the downward transition to lower-tenor Cu-Au mineralization in the central parts of the Aurora zone is inferred to indicate approach to its roots. The potassic-altered phase 2 porphyry hosts scant, sulfide-poor, A-type quartz veinlets, in which pyrite is dominant; however, where this downward transition is abrupt, late-intermineral phase 3 porphyry predominates and locally contains muscovite-bearing quartz veinlets akin to the coarse-grained muscovitic veins in the roots of some Arizona porphyry Cu deposits (e.g., Runyon et al., 2019). The apparent downward weakening of porphyry Cu-Au mineralization due to decreased sulfide content and increased pyrite/chalcopyrite ratios is observed in several other porphyry Cu-Au deposits, including Batu Hijau, Indonesia (Setyandhaka et al., 2008; Schirra et al., 2022), and H14-H15 at Reko Diq, Pakistan (J. Perelló, unpub. data, 2008; Razique et al., 2016); however, at Aurora it is a product of prograde magmatic fluid evolution rather than retrograde fluid ingress as described at Batu Hijau (Schirra et al., 2022).

Lithocap and high-sulfidation epithermal Cu-Au-Ag mineralization

Geologic evidence shows that the advanced argillic lithocap at Filo del Sol largely formed by overprinting of the potassic alteration and associated mineralization during extreme telescoping of the hydrothermal system. Progressive overprinting resulted in partial to complete destruction of earlier-formed, intermediate sulfidation-state, chalcopyrite-pyrite assemblages by high sulfidation-state Cu sulfides and Cu-As sulfosalts (e.g., Sillitoe, 1995; Einaudi et al., 2003; Hedenquist and Arribas, 2022). Although sulfide reconstitution and, hence, recycling of preexisting metals must have taken place early during telescoping (cf. Brimhall, 1979), it appears that all the As in Cu-As sulfosalts and pyrite as well as appreciable amounts of Cu, Au, and Ag must have been introduced by a fluid that followed the residual quartz and quartz-alunite overprint, giving rise to hypogene enrichment of Cu, Au, and Ag (cf. Sillitoe, 1995). Indeed, Cu and Au grades almost doubled during the high-sulfidation event, and the Ag contents, mostly incorporated in numerous Ag-bearing sulfides and sulfosalts, were multiplied several times and reached two orders of magnitude higher concentration than those in pristine potassic alteration (Figs. 2d, 11) even beyond the upper Ag-rich zone. This conclusion is further supported by the presence of a relatively large body of phreatic breccia emplaced during advanced argillic alteration, between successive pulses of high-sulfidation sulfide mineralization. The breccia, confined to the advanced argillic zone, was emplaced relatively late in system evolution, as evidenced by abundant A-type quartz-veinlet and high-sulfidation sulfide clasts, paucity of crosscutting quartz veinlets, and presence of numerous, throughgoing, high-sulfidation veinlets and massive sulfide veins, both accompanied by an equal abundance of disseminated sulfides (Figs. 6, 11). The breccia likely formed by fluid overpressurization at the base of the lithocap (e.g., Sillitoe, 1985, 2010), because a direct relationship with a porphyry intrusion is lacking. Nonetheless, the likely juvenile, tuffaceous and wispy feldspar porphyry components present locally imply a phreatomagmatic origin for parts of the breccia. Development of the currently observed Filo del Sol system concluded with establishment of a relatively shallow, steam-heated zone above the paleogroundwater table. Basal parts of the steam-heated zone overprinted preexisting residual quartz and quartz-alunite, which themselves had already overprinted the A-type quartz-veinlet stockworks (Fig. 11). The steam-heated alteration seems to have removed preexisting Cu and Au, presumably by dispersion into the paleogroundwater system, but introduced native S and cinnabar.

Temporal porphyry Cu development

Miocene magmatism along the Filo del Sol alignment began with emplacement of at least one precursor mafic phase at

15.8 Ma, which is texturally and compositionally indistinguishable from other premineral mafic dikes in the area (Figs. 11, 12b). Pulsed intrusion in short succession (cf. Large et al., 2021) of the three porphyry Cu-bearing phases at Filo del Sol, and elsewhere along the Filo del Sol alignment, followed almost immediately thereafter, at 15.6 Ma, and lasted until at least 15.0 Ma. Porphyry-related magmatism must have extended to ~14.3 Ma, considering the youngest zircon populations present in all dated samples, implying ~1.3 m.y. of zircon crystallization and intrusive activity. This interval is further expanded by the 15.1- to 14.1-Ma Re-Os molybdenite ages for the principal Cu- and Au-bearing porphyry and high-sulfidation mineralization in the Aurora zone at Filo del Sol (~14.7–14.4 Ma) and other centers at Refugio and La Bonita (Figs. 1b, 4, 12b). The U-Pb and Re-Os data for Filo del Sol confirm the rapidity of the hydrothermal telescoping of the system, with overprinting of potassic alteration and related chalcopyrite mineralization in close succession by residual quartz alteration and subsequent high-sulfidation-state sulfide associations (Fig. 13). This rapid evolution at Filo del Sol is further emphasized by a 13.9-Ma K-Ar age for alunite from the lithocap and two K-Ar ages of alunite from the steam-heated zone, which document condensation of H_2S-bearing vapor above the paleogroundwater table at ~13 to 12 Ma. The possibility that the telescoped advanced argillic alteration at Filo del Sol is related to a still-deeper porphyry intrusion has been considered, but to date no evidence for its existence in the form of a second generation of crosscutting potassic alteration and associated mineralization has been encountered, at least to the depth of ~1,900 m explored so far.

The geochronologic data reported, in combination with those from publicly available studies (Devine et al., 2019), suggest that individual mineralized porphyry centers along the Filo del Sol alignment become progressively younger northward, with Tamberías and Vicuña at the southern end being older (16–15 Ma) than those farther north at Filo del Sol, Refugio, and La Bonita (15–14 Ma; Figs. 1b, 4). This northward younging correlates with observed erosion level, with the older porphyry intrusions and related mineralization to the south being exposed and the younger ones farther north still concealed beneath premineral country rocks.

Timing of regional deformation events

The main unconformity preserved in the Filo del Sol area, between the Late Cretaceous volcano-sedimentary unit and the Permo-Triassic basement, may be correlated with the regional unconformity between Late Cretaceous synorogenic strata and Triassic volcanic rocks at the same latitude in Chile. The unconformity marks an important contractional deformation and corresponding erosional event in response to a Late Cretaceous orogenic pulse, which is generally correlated with the Peruvian phase that initiated Andean orogeny (Fig. 12a; e.g., Martínez et al., 2016, and references therein). Although not clearly established in the Filo del Sol area, a second important regional compressive event, recognized in contiguous parts of Chile (Salazar and Coloma, 2016; Rossel et al., 2018; Mpodozis et al., 2018), was associated with the regional Incaic orogenic phase in the middle Eocene to early Oligocene (~42–30 Ma; e.g., Maksaev and Zentilli, 1999), during which porphyry Cu-Au mineralization took place west of the Vicuña belt (e.g., Perelló et al., 1996). In the Filo del Sol area, the late Eocene (35 Ma) porphyry Cu-Au prospect at Flamenco (Figs. 1b, 12) is a probable representative of this phase. A third regional deformation event during the late Oligocene to earliest Miocene at ~26–24 Ma (Fig. 11a; Salazar and Coloma, 2016; Mpodozis et al., 2018) is recorded at Josemaría (Sillitoe et al., 2019). Finally, reverse motion along the El Potro and similar regional faults controlling uplift and denudation of large basement blocks commenced at ~20 Ma in the earliest Miocene (Fig. 12a; Salazar and Coloma, 2016; Rossel et al., 2018; Mpodozis et al., 2018), with demonstrable easterly migrating deformation and basement-block uplift continuing to at least ~13 to 12 Ma a few kilometers south of the Filo del Sol area in Chile (Salazar and Coloma, 2016; Rossel et al., 2018; Fig. 12a). Given their easterly position within the Frontal Cordillera, it is inferred that the regional, basement block-bounding reverse faults that transect the Vicuña belt (e.g., Ventana and Los Helados faults; Fig. 3) were also active during the middle Miocene, at ~14 Ma.

Tempo of hydrothermal telescoping at Filo del Sol

Current evidence indicates that the composite Filo del Sol porphyry Cu-Au and high-sulfidation Cu-Au-Ag system, as well as other centers along the Filo del Sol alignment, were localized by a N- to NE-striking fault zone affecting Permo-Triassic basement rocks (Fig. 13). The structure, probably a steeply W-dipping reverse fault with west-over-east motion, established the weakness zone that later facilitated the premineral mafic intrusions as well as porphyry emplacement. The timing of this master fault at Filo del Sol is unconstrained, but mylonitic rock within it is cut by the premineral mafic dikes which, in turn, are cut by the porphyry intrusions. Because the basement block-bounding reverse faults transecting the Vicuña belt were active in the middle Miocene, at ~14 to 12 Ma, it is inferred that this controlling structure at Filo del Sol was also undergoing reverse motion and causing basement uplift at the same time, in effect during porphyry Cu-Au formation (Fig. 13).

As a direct result of the middle Miocene contractional deformation and consequent uplift of basement-cored blocks under a dominantly thick-skinned structural regime, the porphyry Cu-Au system at Filo del Sol underwent intense synmineral erosion and exhumation, resulting in progressive paleosurface degradation and consequent alteration-mineralization telescoping (e.g., Sillitoe, 1994). An epithermal overprint was rapidly established in what was previously a deeper-level potassic alteration zone, and several pulses of high-sulfidation mineralization as well as intervening phreatic (and likely phreatomagmatic) breccia bodies were emplaced (Fig. 13). This situation is reminiscent of the giant porphyry Cu deposits of the middle Eocene to early Oligocene belt of northern Chile, some of which display telescoping of structurally localized high-sulfidation mineral assemblages over deeper alteration types (Sillitoe and Perelló, 2005).

Similarly, the lack of coeval volcanism of 14 to 12-Ma age along the Vicuña belt is consistent with the contractional tectonism during porphyry Cu-Au formation along the Filo del Sol alignment. Indeed, suppression of volcanism during compression accompanied by high rates of surface uplift and rapid exhumation are considered to provide the optimal con-

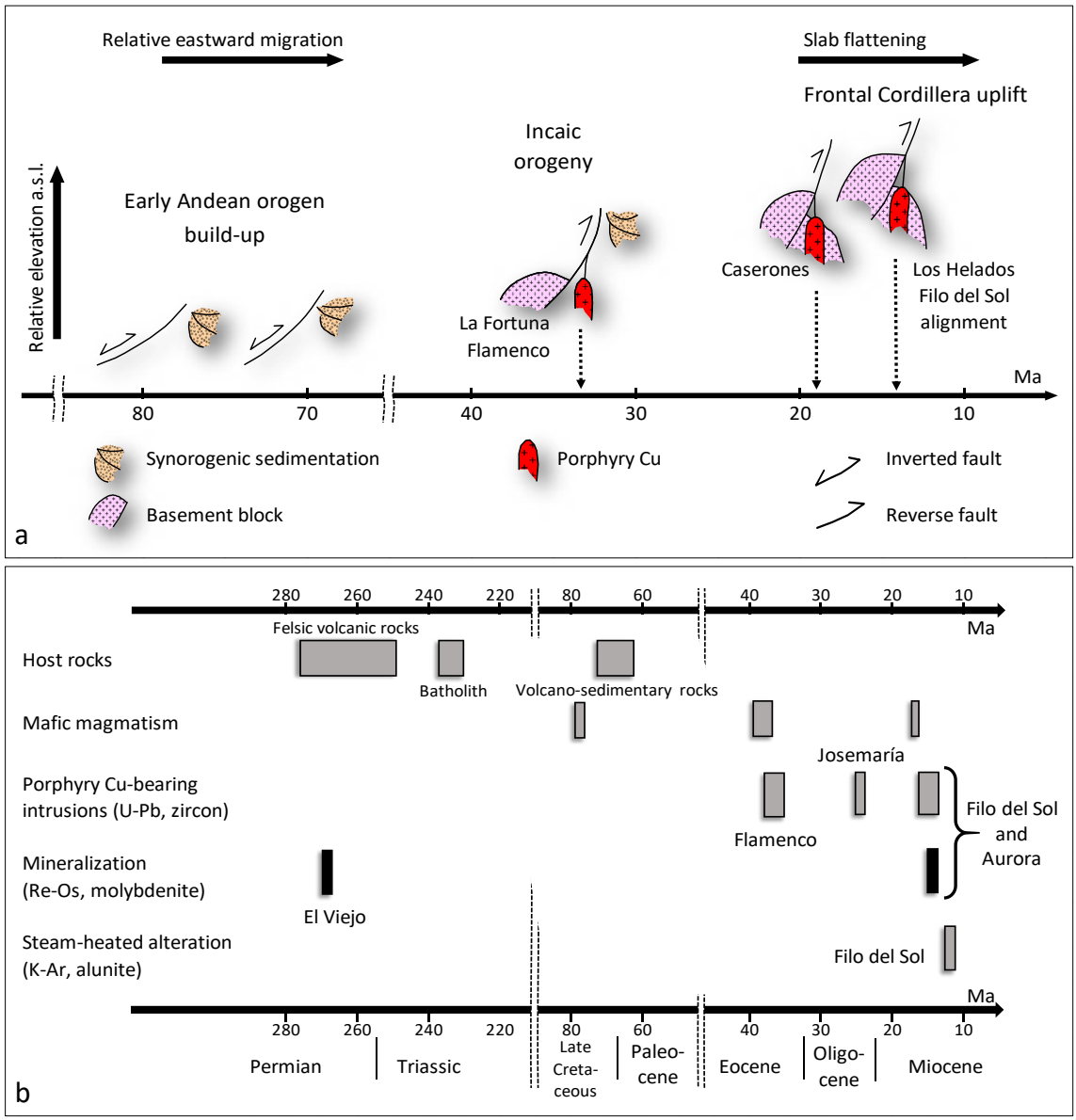

Fig. 12. Summary chronology of selected regional tectono-magmatic events. a. Schematic representation of events at latitude of Vicuña belt. Note eastward migration of deformation, magmatism, and porphyry Cu mineralization and corresponding cumulative uplift. b. Chart displaying timing of principal porphyry Cu-bearing intrusions and mineralization, including recurrent porphyry Cu events at Permian El Viejo and Eocene Flamenco centers. Note precursor mafic intrusion at Filo del Sol and molybdenite mineralization at end of a ~1-m.y. porphyry Cu intrusion event.

ditions for accumulation of fluid-rich magma in large, shallow-level reservoirs propitious for giant porphyry Cu development (e.g., Sillitoe, 1998), as exemplified by the most productive porphyry Cu belts of the central Andes (Sillitoe and Perelló, 2005).

Rapid erosional unroofing at Filo del Sol was presumably accompanied by development of a sequence of steam-heated zones above paleogroundwater tables, the youngest of which is still partially preserved (Fig. 13). The age of hypogene alunite from this zone, ranging from ~13 to 12 (±1–2) Ma, constrains the timing of paleosurface formation in the Filo del Sol area, and supports correlation with coeval paleosurfaces established elsewhere in the region, particularly the Azufreras-Torta paleosurface at elevations of ~5,000 m in the El Indio belt ~80–100 km farther south (Bissig et al., 2002). The time elapsed between formation of the porphyry-related quartz veinlets and establishment of the partly preserved steam-heated zone could have been as little as ~1 m.y., thereby implying a short-lived duration of erosion for the entire system. Exhumation at Filo del Sol was perhaps twice as fast as it was ~10 m.y. earlier (~24 Ma) at the nearby Josemaría porphyry Cu-Au deposit, the latter estimated to have been unroofed at rates in the 0.5 km/m.y. range (Sillitoe et al., 2019). If similar parameters are applied to Filo del Sol, a lithocap column of ~1,000 m was removed during the 1 m.y. period of porphyry evolution and telescoping, indicating a much faster exhumation rate than the average estimate for porphyry Cu deposits worldwide (158 m/m.y.; Kesler and Wilkinson, 2006).

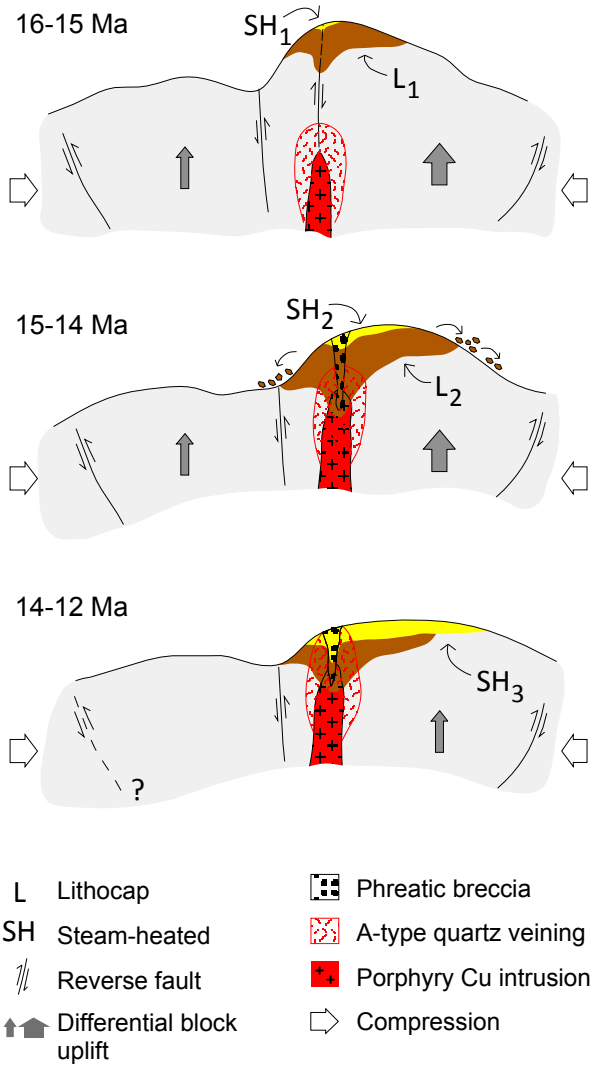

Fig. 13. Schematic evolution of Filo del Sol porphyry-epithermal deposit in a broadly west-to-east, N-looking cross section, showing reverse fault-controlled disposition of Permian-Triassic rocks within regional-scale, pop-up basement-cored block delimited by regional reverse faults (e.g., El Potro in Chile and Mogotes in Argentina, as shown in Fig. 3b). Differential uplift between blocks is emphasized by arrows. Structural panel hosting telescoped porphyry-epithermal system at Filo del Sol is inferred to have undergone higher rate of synmineral uplift and denudation than adjacent blocks to west and east. See text for further discussion.

Although porphyry-related lithocaps and telescoped porphyry systems of various ages are common in the Frontal Cordillera and Sierras Pampeanas of the southern Central Andes (e.g., Perelló et al., 1996, 1998; Bissig et al., 2001; Sillitoe et al., 2016), preservation of the paleosurface and advanced argillic lithocap at Filo del Sol is intriguing given the high rates of surface uplift and rapid denudation experienced by the basement blocks. Concealment beneath postmineral cover, which is one way to enhance porphyry Cu preservation, as at Josemaría (Sillitoe et al., 2019) and elsewhere in the world (e.g., Manske and Paul, 2002; Braxton et al., 2012), does not apply at Filo del Sol, although the system could have been protected from erosion in a structurally controlled panel undergoing less-pronounced uplift than adjoining blocks. Indeed, the broadly contemporaneous Tamberías porphyry Cu-Au prospect, immediately to the south (Figs. 1b, 4), was almost entirely unroofed during the same period, with its potassic core and associated quartz-veinlet stockworks now exposed at surface (Fig. 7). Clearly, structural compartmentalization along the Filo del Sol alignment must have played a role during porphyry Cu emplacement and subsequently, with differential uplift characterizing contiguous blocks: a condition that may well be relatively common in porphyry Cu districts (e.g., Perelló et al., 1996, 2018; Hervé et al., 2012; Sillitoe et al., 2016).

Evidence from Filo del Sol (this study), the nearby Josemaría deposit (Sillitoe et al., 2019), and other deposits and prospects in the region (Perelló et al., 1996, 1998) demonstrates that porphyry Cu deposits formed in magmatic arc terranes undergoing contractional tectonism and rapid rock uplift can be unroofed in 1 to 2 m.y. under a range of climatic regimes (cf. Sillitoe et al., 2019), and presumably due to maximization of erosion rates following major pulses of Andean uplift (Carretier et al., 2015).

Metallogenic implications and porphyry Cu recurrence

The Filo del Sol alignment has been the site of porphyry Cu mineralization events in the late Paleozoic, late Eocene, and middle Miocene (Fig. 12b). The 266-Ma El Viejo prospect is overprinted by parts of the Filo del Sol lithocap and related high-sulfidation Cu-Au-Ag mineralization (Figs. 1b, 4), whereas at Flamenco, a block of 35-Ma porphyry and associated Cu-Au-bearing quartz-veinlet stockwork occurs alongside the larger, 16 to 15-Ma Tamberías porphyry Cu-Au system.

Similar recurrence of porphyry Cu mineralization is known elsewhere in the southern Central Andes. A productive, albeit small porphyry Cu system of Early Permian age (290–285 Ma) was overprinted by the much larger, late Eocene porphyry Cu-Mo-Au mineralization at the Zaldívar deposit in the Escondida district (Perelló et al., 2018), and middle Permian Re-Os ages (265 and 256 Ma) were obtained for molybdenite from porphyry-related quartz veinlets in a porphyry prospect in the late Eocene Collahuasi-Quebrada Blanca district (Munizaga et al., 2008), both along the northern Chile porphyry Cu belt (Sillitoe and Perelló, 2005). In the Frontal Cordillera of San Juan province, Argentina, the late Miocene (10–9 Ma) Morro del Cobre (Bastías Torres et al., 2021) and Early Permian (280 Ma) Yalguaraz (Sillitoe, 1977; Torres et al., 2020) porphyry Cu prospects also occur adjacent to one another. Several other cases exist in the Andes of Peru and Ecuador (J. Perelló, unpub. data, 2022), implying that some kind of fundamental, most likely deep-seated and long-lived, features must have controlled the sites of porphyry Cu emplacement during construction of superposed Andean orogens.

Supergene aspects

Although present throughout the shallow parts of the Filo del Sol system, supergene Cu mineralization developed preferentially in the central and southern parts, coincident with the surficial chalcanthite and the bulk of the oxidized resource (Devine et al., 2019; Figs. 1c, 2d). The supergene mineralization is mainly in the form of chalcanthite, although structural and hydrothermal breccia zones focused local descent of Cu-charged solutions to form irregular and immature zones of

supergene chalcocite enrichment. In contrast, within the rest of the system, particularly where the lithocap and steam-heated alteration are superimposed, the leached zone is barren of metals and underlain by a thin, irregular zone of mixed oxide- and sulfide-bearing Cu minerals at the transition from supergene- to hypogene-dominated environments. In combination, these features strongly suggest that the bulk of the supergene profile developed relatively recently, although the precise timing remains unknown. Erosional unroofing of the deposit and initiation of supergene activity must have taken place after establishment of the steam-heated zone and concurrently with continued late Miocene uplift of the large basement block in which Filo del Sol is located. A Pliocene timing is inferred on the basis of supergene ages from the topographically elevated Sierras Pampeanas at Agua Rica (3.9 Ma; Perelló et al., 1998), and Sierras de Famatina at Famatina (~3 Ma; Sillitoe, 2005), as well as in the glaciated landscape farther south in central Chile at Los Pelambres (3–1 Ma; Perelló et al., 2012). Clearly, supergene processes were active prior to the Late Glacial Maximum at ~13,000 ^{14}C yr B.P. (Geyh et al., 1999; Ammann et al., 2001), because leached capping material was incorporated in periglacial deposits and preserved under present-day glaciers (Perucca and Angillieri, 2008), which are unmelted remnants of the more extensive Holocene glacial cover (Fig. 3). The abundance of ephemeral chalcanthite, water-soluble Fe sulfates, and ilsemannite shows that supergene processes in the acidic environment of the Filo del Sol area remain active, except when all water is frozen during winter seasons, as they are elsewhere in the southern Central Andes (Sillitoe, 2005).

The distribution of the high-grade (>60 ppm) Ag mineralization is tentatively explained in terms of a combination of hypogene and supergene processes, whereby the hypogene, Ag-bearing sulfide and sulfosalt species generated in the upper parts of the high-sulfidation lodes were later partially modified by supergene processes under the prevailing arid and sulfate-rich acidic conditions. This interpretation accords with the mixed hypogene and supergene Ag mineralogy and suggests that much of the oxidation occurred essentially in situ (cf. Sillitoe, 2009), although localized Ag mobilization and reprecipitation undoubtedly also took place. Original host-rock permeability, provided either by specific siliciclastic horizons in the Late Cretaceous sequence or the granular matrix of phreatic breccias, promoted lateral and/or vertical fluid transport and provided preferred sites for the original hypogene and later supergene mineralization.

Comparisons

Filo del Sol geology is similar to that of several other deposits characterized by the presence of advanced argillic alteration and high-sulfidation mineralization, including Pascua-Lama in the El Indio belt and Agua Rica in the northernmost Sierras Pampeanas—both like Filo del Sol in rapidly uplifted basement-cored blocks, as well as Onto, in the still-active Sunda island arc, Indonesia, and Resolution in the Laramide province of Arizona.

The Pascua-Lama high-sulfidation epithermal Au-Ag deposit is centered on a large hydrothermal breccia body that was emplaced during advanced argillic alteration and high-sulfidation mineralization (Chouinard et al., 2005). It may be compared with the phreatic breccia at Filo del Sol, both in style and intermineral timing. Like Filo del Sol, Pascua-Lama retains part of its superjacent steam-heated zone and contains a shallow, subhorizontal zone of elevated Ag values that appears to have formed late in the high-sulfidation stage (Chouinard et al., 2005). Dominant chlorargyrite in the Ag zone is likely a supergene weathering product of pre-existing Ag sulfides and sulfosalts rather than hypogene as proposed by Chouinard et al. (2005). Based on these analogous features, it seems certain that porphyry intrusions and associated potassic alteration and accompanying Cu-Au mineralization exist at depth (cf. Chouinard et al., 2005), although the degree of telescoping is appreciably less, probably because Pascua-Lama was formed at ~8 Ma (Bissig et al., 2001), after compressive tectonism and concomitant uplift in the El Indio belt had given way to strike-slip faulting (Giambiagi et al., 2017).

The Agua Rica Cu-Au-Mo deposit comprises potassic-altered porphyry intrusions and associated pyrite-chalcopyrite-molybdenite overprinted by a zone of advanced argillic alteration and high-sulfidation pyrite-covellite-enargite, much of it confined to an intermineral hydrothermal breccia (Perelló et al., 1998; Landtwing et al., 2002; Franchini et al., 2011). Erosion is deeper than at Filo del Sol, as shown by the minor development of vuggy residual quartz and absence of an overlying steam-heated zone. Telescoping is extreme, as at Filo del Sol, because compressive tectonism, uplift, and exhumation were contemporaneous with deposit formation at ~6.5 Ma (Perelló et al., 1998; Borba et al., 2020).

The Onto composite porphyry-epithermal Cu-Au deposit is comparable to Filo del Sol in having an early potassic zone and associated chalcopyrite mineralization extensively overprinted by quartz-pyrophyllite-alunite and shallower quartz-pyrite alteration and associated high-sulfidation mineralization dominated by pyrite and covellite, all part of an areally extensive lithocap (Burrows et al., 2020). The entire Onto deposit was emplaced beneath an andesitic flow unit that appears to have acted as an impermeable barrier (Burrows et al., 2020). Although the porphyry intrusions, magmatic-hydrothermal breccia, and potassic alteration at Filo del Sol were largely confined beneath a sill, the phreatic breccia and residual quartz and quartz-alunite alteration breached this lithologic seal and approached the paleosurface as evidenced by the steam-heated zone. In contrast, the capping flow at Onto may have prevented significant vapor ascent to the vadose zone and development of widespread steam-heated alteration. Therefore, the extreme alteration-mineralization telescoping at Onto was caused by reactive, high sulfidation-state fluids being impounded beneath the capping andesite rather than, as in most cases, including Filo del Sol, by rapid exhumation.

Resolution, a deep, high-grade, hypogene porphyry Cu-Mo deposit, has some obvious geologic similarities to Filo del Sol, namely, the linear trend of porphyry intrusions controlled by preexisting faults (Hehnke et al., 2012); telescoping of strong hydrolytic alteration comprising upward-flared quartz-sericite-pyrite-chalcopyrite-bornite and high sulfidation-state (pyrite-chalcocite-digenite-bornite) associations over earlier-formed potassic alteration (J. Perelló, unpub. report, 1997; Manske and Paul, 2002); Cu mineralization straddling an unconformity between basement and Cretaceous cover

rocks (Manske and Paul, 2002; Hehnke et al., 2012); lower Cu tenor of intermineral porphyry dikes relative to contiguous host rocks; and high-grade bodies of synmineral magmatic-hydrothermal breccia. There are, however, several notable differences; mafic dikes and sills at Filo del Sol did not act to localize high-grade ore like the Proterozoic diabase sills at Resolution and mafic host rocks elsewhere (Sillitoe, 2010), perhaps because those at Filo del Sol occur on the margins of the deposit; absence at Filo del Sol of the quartz-sericite-pyrite-chalcopyrite-bornite assemblage that introduced much of the Cu at Resolution (Hehnke et al., 2022); and lesser importance of synmineral telescoping and hypogene metal enrichment at Resolution, although much of its lithocap appears to have been eroded before burial beneath postmineral sedimentary and volcanic cover.

Conclusions

The Filo del Sol Cu-Au-Ag deposit is a particularly well-preserved example of a highly telescoped porphyry Cu system in which the lithocap environment overprints a sequence of porphyry intrusions, a large, intermineral, magmatic-hydrothermal breccia body, and associated potassic alteration and accompanying chalcopyrite-pyrite mineralization. Sulfide and chalcopyrite contents diminish downward in the potassic zone, heralding approach to the bottom of the mineralized zone. At Filo del Sol, the lithocap consists of at least one large and several smaller, steeply inclined zones of vuggy residual quartz and intense silicification that are separated by and grade outward to a quartz-alunite assemblage and subsidiary peripheral aluminosilicate alteration. Phreatic brecciation was active during this overprint event. Several styles of pyrite and early enargite followed by Cu sulfides and numerous Ag-bearing species constitute the accompanying high-sulfidation mineralization. The composite vuggy residual quartz and quartz-alunite alteration host the highest Cu and Au grades. Notwithstanding the high uplift rate, ~1 km/m.y., that prevailed during deposit formation, a shallow zone of largely barren, steam-heated alteration generated above the paleogroundwater table is extensively preserved. Therefore, the full vertical extent of the Filo del Sol system, from the steam-heated zone at the top to weakly mineralized potassic zone at the bottom, is only ~1.5 km, which shows how extreme telescoping can result not only in hypogene enrichment of Cu, Au, and Ag but also in vertically compressed systems. In combination, these two parameters make telescoped porphyry Cu-Au systems particularly attractive exploration targets.

Acknowledgments

This paper is the product of hard field work and incremental interpretative advances by many geologists over the past two decades. Early input by the late Peter Drobeck as well as Patricio Jones, Ricardo Martínez, Alfredo Vitaller, Martín Rode, Max La Motte, Jorge Achem, Federico Fuentes, Martin Sanguinetti, Fernando Richard, Juan Arrieta, Agustin Guitart, Emilio Fernández, and Leo Ortíz deserve special mention. More recently, geologic work by Leticia González, Aylen Tremea, Candela Becerra, Lucas Cataldi, Nerea Fuentes, Lucio Simoncini, Juan Sabadín, Jimena López, Federico Monfort, and Julieta González, as well as the efforts of the technical support staff, have been critical for project advancement. Rob Creaser and Victor Valencia are thanked for provision of the Re-Os and U-Pb ages, respectively. Contributions by Fionnuala Devine, Giovanni Di Prisco, Dave Heberlein, and William Kerby as well as management guidance and support from Jaime Beck, Bob Carmichael, and Wojtek Wodzicki are also gratefully acknowledged. Bob Carmichael also promptly granted permission for manuscript publication. Review comments by Constantino Mpodozis, Bob Carmichael, and, on behalf of *Economic Geology*, Bill Chávez and Jeff Hedenquist led to improvement of the manuscript. Finally, we acknowledge the major contribution of the late Lukas Lundin, who believed enough in the Filo del Sol project to enthusiastically support the exploration programs, both financially and spiritually, from acquisition through to discovery of the Aurora zone. The level of support, persistence, and belief that Lukas held for this project is rare in management and a key factor in the discovery.

REFERENCES

Ammann, C., Bettina, J., Kammer, K., and Messerli, B., 2001, Late Quaternary glacier response to humidity changes in the arid Andes of Chile (18–29°S): Palaeogeography, Palaeoclimatology, Palaeoecology, v. 172, p. 313–326.

Anderson, M., Alvarado, P., Zandt, G., and Beck, S., 2007, Geometry and brittle deformation of the subducting Nazca plate, Central Chile and Argentina: Geophysical Journal International, v. 171, p. 419–434.

Bastías-Mercado, F., González, J., and Oliveros, V., 2020, Volumetric and compositional estimation of the Choiyoi Magmatic Province and its comparison with other Silicic Large Igneous Provinces: Journal of South American Earth Sciences, v. 103, 102749, doi.org/10.1016/j.jsames.2020.102749.

Bastías Torres, M.V., Rubinstein, N., Previley, L., and Poole, G., 2021, Petrogenesis of the Miocene Morro del Cobre Cu (Mo)-porphyry deposit in the Frontal Cordillera over the Pampean flat-slab segment, Argentina: Journal of South American Earth Sciences, v. 110, 103343, doi.org/10.1016/j.jsames.2021.103343.

Bissig, T., Lee, J.K.W., Clark, A.H., and Heather, K.B., 2001, The Cenozoic history of volcanism and hydrothermal alteration in the Central Andean Flat-Slab Region: New ^{40}Ar-^{39}Ar constraints from the El Indio–Pascua Au (-Ag, Cu) belt, 29°20′–30°30′ S: International Geology Review, v. 43, p. 312–340.

Bissig, T., Clark, A.H., Lee, J.K.W., and Hodgson, C.J., 2002, Miocene landscape evolution and geomorphologic controls on epithermal processes in the El Indio-Pascua Au-Ag-Cu belt, Chile and Argentina: Economic Geology, v. 97, p. 971–996.

Borba, M.L., Tassinari, C.C.G., Kirk, J., and Ruiz, J., 2020, Ages and isotope evolution of the Agua Rica Cu-Au porphyry-epithermal deposit, NW Argentina: Ore Geology Reviews, v. 119, 103395, doi.org/10.1016/j.oregeorev.2020.103395.

Braxton, D.P., Cooke, D.R., Dunlap, J., Norman, M., Reiners, P., Stein, H., and Waters, P., 2012, From crucible to graben in 2.3 Ma: A high-resolution geochronological study of porphyry life cycles, Boyongan-Bayugo copper-gold deposits, Philippines: Geology, v. 40, p. 471–474.

Brimhall, G.H., Jr., 1979, Lithologic determination of mass transfer mechanisms of multiple-stage porphyry copper mineralization at Butte, Montana: Vein formation by hypogene leaching and enrichment of potassium-silicate protore: Economic Geology, v. 74, p. 556–589.

Buret, Y., von Quadt, A., Heinrich, C., Selby, D., Wälle, M., and Peytcheva, I., 2016, From a long-lived upper-crustal magma chamber to rapid porphyry copper emplacement: Reading the geochemistry of zircon crystals at Bajo de la Alumbrera (NW Argentina): Earth and Planetary Science Letters, v. 450, p. 120–131.

Burrows, D.R., Rennison, M., Burt, D., and Davies, R., 2020, The Onto Cu-Au discovery, eastern Sumbawa, Indonesia: A large, middle Pleistocene lithocap-hosted high-sulfidation covellite-pyrite porphyry deposit: Economic Geology, v. 115, p. 1385–1412.

Cahill, T., and Isacks, B.L., 1992, Seismicity and shape of the subducted Nazca plate: Journal of Geophysical Research, v. 97, B12, p. 17,503–17,529.

Calder, M.F., Chang, Z., Arribas, A., Gaibor, A., Dunkley, P., Pastoral, J., Kouzmanov, K., Spandler, C., and Hedenquist, J.W., 2022, High-grade

copper and gold deposited during postpotassic chlorite-white mica-albite stage in the Far Southeast porphyry deposit, Philippines: Economic Geology, v. 117, p. 1573–1596.
Carretier, S., Tolorza, V., Rodríguez, M.P., Pepin, E., Aguilar, G., Regard, V., Martinod, J., Riquelme, R., Bonnet, S., Brichau, S., Hérail, G., Pinto, L., Farías, M., Charrier, R., and Guyot, J.L., 2015, Erosion in the Chilean Andes between 27°S and 39°S: tectonic, climatic and geomorphic control: Geological Society, London, Special Publications 399, p. 401–418.
Charchaflié, D., and Gray, J., 2014, Initial mineral resource estimate for the Filo del Sol property, Region III of Atacama, Chile and San Juan Province, Argentina: NI 43-101 Technical Report prepared for NGEx Resources Inc., 107 p., www.filo-mining.com.
Charchaflié, D., Tosdal, R.M., and Mortensen, J.K., 2007, Geologic framework of the Veladero high-sulfidation epithermal deposit area, Cordillera Frontal, Argentina: Economic Geology, v. 102, p. 171–192.
Charchaflié, D., Rossello, J., Richard, F., González Castellote, L., Arrieta, J., and Sanguinetti, M., 2019, Filo del Sol project, the discovery of an intricate Miocene porphyry/epithermal system in the Argentina-Chile Andes [ext. abs.]: Society of Economic Geologists Conference, 2019, South American Metallogeny: Sierra to Craton: Santiago, Chile, CD-ROM, 4 p.
Chouinard, A., Williams-Jones, A.E., Leonardson, R.W., Hodgson, C.J., Silva, P., Téllez, C., Vega, J., and Rojas, F., 2005, Geology and genesis of the multistage high-sulfidation epithermal Pascua Au-Ag-Cu deposit, Chile and Argentina: Economic Geology, v. 100, p. 463–490.
del Rey, A., Deckart, K., Planavsky, N., Arriagada, C., and Martínez, F., 2019, Tectonic evolution of the southwestern margin of Pangea and its global implications: Evidence from the mid Permian–Triassic magmatism along the Chilean-Argentine border: Gondwana Research, v. 76, p. 303–321.
Devine, F., Charchaflié, D., and Gray, J.N., 2015, Updated mineral resource estimate for the Filo del Sol property, Region III of Atacama, Chile and San Juan Province, Argentina: NI 43-101 Technical Report prepared for NGEx Resources Inc., 103 p., www.filo-mining.com.
Devine, F., Charchaflié, D., and Gray, J.N., 2016, Geological report for the Filo del Sol property, Region III, Chile and San Juan Province, Argentina: NI 43-101 Technical Report prepared for Filo Mining Corp., 93 p., www.filo-mining.com.
Devine, F., Charchaflié, D., Di-Prisco, G., and Gray, J.N., 2017, Resource update report for the Filo del Sol property, Region III, Chile and San Juan Province, Argentina: NI 43-101 Technical Report prepared for Filo Mining Corp., 218 p., www.filo-mining.com.
Devine, F., Kalanchey, R., Winkelmann, N., Gray, J., Melnyk, J., Elfen, S., Borntraeger, B., and Stillwell, I., 2019, NI 43-101 Technical Report, prefeasibility study for the Filo del Sol project: Vancouver, Canada, Ausenco Services, 261 p., www.filo-mining.com.
Einaudi, M.T., Hedenquist, J.W., and Inan, E.E., 2003, Sulfidation state of fluids in active and extinct hydrothermal systems: Transitions from porphyry to epithermal environments: Society of Economic Geologists Special Publication 10, p. 285–313.
Franchini, M., Impiccini, A., Lentz, D., Ríos, F.J., O'Leary, S., Pons, J., and Schalamuk, A.I., 2011, Porphyry to epithermal transition in the Agua Rica polymetallic deposit, Catamarca, Argentina: An integrated petrologic analysis of ore and alteration parageneses: Ore Geology Reviews, v. 41, p. 49-74
Franchini, M., McFarlane, C., Maydagán, L., Reich, M., Lentz, D.R., Meinert, L., and Bouhier V., 2015, Trace metals in pyrite and marcasite from the Agua Rica porphyry-high sulfidation epithermal deposit, Catamarca, Argentina: Textural features and metal zoning at the porphyry to epithermal transition: Ore Geology Reviews, v. 66, p. 366–387.
Frikken, P.H., Cooke, D.R., Walshe, J.L., Archibald, D., Skarmeta, J., Serrano, L., and Vargas, R., 2005, Mineralogical and isotopic zonation in the Sur-Sur tourmaline breccia, Río Blanco-Los Bronces Cu-Mo deposit, Chile: Implications for ore genesis: Economic Geology, v. 100, p. 935–961.
Geyh, M.A., Grosjean, M., Núñez, L., and Schotterer, U., 1999, Radiocarbon reservoir effect and the timing of the late-glacial/early Holocene humid phase in the Atacama Desert (Northern Chile): Quaternary Research, v. 52, p. 143–153.
Giambiagi, L., Álvarez, P.P., Creixell, C., Mardonez, D., Murillo, I., Velásquez, R., Lossada, A., Suriano, J., Mescua, J., and Barrionuevo, M., 2017, Cenozoic shift from compression to strike-slip stress regime in the high Andes at 30°S, during the shallowing of the slab: Implications for the El Indio/Tambo mineral district: Tectonics, v. 36, p. 2714–2735.
Giambiagi, L., Tassara, A., Echaurren, A., Julve, J., Quiroga, R., Barrionuevo, M., Sibiao, L., Echeverría, I., Mardónez, D., Suriano, J., Mescua, J., Lossada, A.C., Spagnotto, S., Bertoa, M., and Lothari, L., 2022, Crustal anatomy and evolution of a subduction-related orogenic system: Insights from the Southern Central Andes (22-35°S): Earth-Science Reviews, 104138, doi.org/10.1016/j.earscirev.2022.104138.
Gianni, G.M., and Navarrete, C.S., 2022, Catastrophic slab loss in southwestern Pangea preserved in the mantle and igneous record: Nature Communications, v. 13, 698, doi.org/10.1038/s41467-022-28290-z.
Guitart, A., 2020, The geology, alteration and timing of porphyry intrusions and breccias associated with the development of Los Helados porphyry copper-gold deposit, Chile: Vancouver, Canada, University of British Columbia, Unpublished MSc thesis, 227 p., doi.10.14288/1.0392531.
Gustafson, L.B., and Hunt, J.P., 1975, The porphyry copper deposit at El Salvador, Chile: Economic Geology, v. 70, p. 857–912.
Hedenquist, J.W., and Arribas, A., 2022, Exploration implications of multiple formation environments of advanced argillic minerals: Economic Geology, v. 117, p. 609–643.
Hedenquist, J.W., and Taran, Y.A., 2013, Modeling the formation of advanced argillic lithocaps: Volcanic vapor condensation above porphyry intrusions: Economic Geology, v. 108, p. 1523–1540.
Hehnke, C., Ballantyne, G., Martin, H., Hart, W., Schwarz, A., and Stein, H., 2012, Geology and exploration progress at the Resolution porphyry Cu-Mo deposit, Arizona: Society of Economic Geologists Special Publication 16, p. 147–166.
Hervé, M., Sillitoe, R.H., Wong, C., Fernández, P., Crignola, F., Ipinza, M., and Urzúa, F., 2012, Geologic overview of the Escondida porphyry copper district, northern Chile: Society of Economic Geologists Special Publication 16, p. 55–78.
Holley, E.A., Bissig, T., and Monecke, T., 2016, The Veladero high-sulfidation epithermal gold deposit, El Indio-Pascua belt, Argentina: Geochronology of alunite and jarosite: Economic Geology, v. 111, p. 311–330.
Jannas, R.R., Bowers, T.S., Petersen, U., and Beane, R.E., 1999, High-sulfidation deposit types in the El Indio district, Chile: Society of Economic Geologists Special Publication 7, p. 219–266.
Jones, J.P., 2007, Exploración minera en la República Argentina, áreas examinadas por Deprominsa: Asociación Argentina de Geólogos Economistas, Publicación Especial 1, p. 10–20.
Jones, J.P., and Martínez, R.D., 2007, Aspectos regionales de nuevos sistemas porfíricos en Argentina, desde Salta hasta Mendoza: Asociación Argentina de Geólogos Economistas, Publicación Especial 1, p. 21–30.
Jordan, T.E., Isacks, B.L., Allmendinger, R.W., Brewer, J.A., Ramos, V.A., and Ando, C.J., 1983, Andean tectonics related to geometry of subducted Nazca plate: Geological Society of America Bulletin, v. 94, p. 341–361.
Kay, S.M., and Mpodozis, C., 2001, Central Andean ore deposits linked to evolving shallow subduction system and thickening crust: GSA [Geological Society of America] Today, v. 11, p. 4–9.
——2002, Magmatism as a probe to the Neogene shallowing of the Nazca plate beneath the modern Chilean flat-slab: Journal of South American Earth Sciences, v. 15, p. 39–57.
Kay, S.M., Ramos, V.A., Mpodozis, C., and Sruoga, P., 1989, Late Paleozoic to Jurassic silicic magmatism at the Gondwana margin: Analogy to the Middle Proterozoic in North America?: Geology, v. 17, p. 324–328.
Kay, S.M., Mpodozis, C., Tittler, A., and Cornejo, P., 1994, Tertiary magmatic evolution of the Maricunga mineral belt in Chile: International Geology Review, v. 36, p. 1079–1112.
Kesler, S.E., and Wilkinson, B.H., 2006, The role of exhumation in the temporal distribution of ore deposits: Economic Geology, v. 101, p. 919–922.
Landtwing, M.R., Dillenbeck, E.D., Leake, M.H., and Heinrich, C., 2002, Evolution of the breccia-hosted porphyry Cu-Mo-Au deposit at Agua Rica, Argentina: Progressive unroofing of a magmatic hydrothermal system: Economic Geology, v. 97, p. 1273–1292.
Large, S.J.E., Wotzlaw, J.-F., Guillong, M., von Quadt, A., and Heinrich, C.A., 2020, Resolving the timescales of magmatic and hydrothermal processes associated with porphyry deposit formation using zircon U-Pb petrochronology: Geochronology, v. 2, p. 209–230.
Large, S.J.E., Buret, Y., Wotzlaw, J.-F., Karakas, O., Guillong, M., von Quadt, A., and Heinrich, C.A., 2021, Copper-mineralised porphyries sample the evolution of a large-volume silicic magma reservoir from rapid assembly to solidification: Earth and Planetary Science Letters, v. 563, 116877, doi.org/10.1016/j.epsl.2021.116877.
Maksaev, V., and Zentilli, M., 1999, Fission track thermochronology of the Domeyko Cordillera, northern Chile: Implications for Andean tectonics and porphyry copper metallogenesis: Exploration and Mining Geology, v. 8, p. 65–89.

Maksaev, V., Moscoso, R., Mpodozis, C., and Nasi, C., 1984, Las unidades volcánicas y plutónicas del Cenozoico superior en la Alta Cordillera del Norte Chico (29°-31°S): Geología, alteración hidrotermal y mineralización: Revista Geológica de Chile, no. 21, p. 11–51.

Maksaev, V., Munizaga, F., and Tassinari, C., 2014, Timing of the magmatism of the paleo-Pacific border of Gondwana: U-Pb geochronology of Late Paleozoic to Early Mesozoic igneous rocks of the north Chilean Andes between 20° and 31°S: Andean Geology, v. 41, p. 447–506.

Manske, S.L., and Paul, A.H., 2002, Geology of a major new porphyry copper center in the Superior (Pioneer) district, Arizona: Economic Geology, v. 97, p. 197–220.

Martin, M., Clavero R., and Mpodozis, C., 1997, Eocene to late Miocene magmatic development of El Indio belt, 30°S, north central Chile [ext. abs.]: Congreso Geológico Chileno, 8th, Antofagasta, 1997, Actas, v. 1, p. 149–153.

Martínez, F., Peña, M., and Arriagada, C., 2015a, Geología de las áreas Iglesia Colorada-Cerro del Potro y Cerro Mondaquita, Región de Atacama. Escala 1:100,000: Servicio Nacional de Geología y Minería, Carta Geológica de Chile, Serie Geología Básica 179–180, 67 p.

Martínez, F., Arriagada, C., Valdivia, R., Deckart, K., and Peña, M., 2015b, Geometry and kinematics of the Andean thick-skinned thrust systems: Insights from the Chilean Frontal Cordillera (28°–28.5°S), Central Andes: Journal of South American Earth Sciences, v. 64, p. 307–324.

Martínez, F., Arriagada, C., Peña, M., Deckart, K., and Charrier, R., 2016, Tectonic styles and crustal shortening of the Central Andes "Pampean" flat-slab segment in northern Chile (27–29°S): Tectonophysics, v. 667, p. 144–162.

Martínez, F., Arriagada, C., and Bascuñán, S., 2018, Mechanisms and episodes of deformation along the Chilean–Pampean flat-slab subduction segment of the Central Andes in northern Chile, *in* Folguera, A., et al., eds., The evolution of the Chilean-Argentinean Andes: Springer Cham, Springer Earth System Sciences, p. 273–290.

McCallum, M.E., 1985, Experimental evidence for fluidization processes in breccia pipe formation: Economic Geology, v. 80, p. 1523–1543.

Meyer, C., 1965, An early potassic type of wall-rock alteration at Butte, Montana: American Mineralogist, v. 50, p. 1717–1722.

Moscoso, R., and Mpodozis, C., 1988, Estilos estructurales en el norte chico de Chile (28-31°S), Regiones de Atacama y Coquimbo: Revista Geológica de Chile, v. 15, no. 2, p. 151–166.

Mpodozis, C., and Kay, S.M., 2003, Neogene tectonics, ages and mineralization along the transition zone between the El Indio and Maricunga mineral belts (Argentina and Chile 28°–29°S) [abs.]: Congreso Geológico Chileno, 10th, Concepción, 2003, CD-ROM, 1 p.

Mpodozis, C., Cornejo, P., Kay, S.M., and Tittler, A., 1995, La franja de Maricunga: Síntesis de la evolución del frente volcánico Oligoceno-Mioceno de la zona sur de los Andes Centrales: Revista Geológica de Chile, v. 21, no. 2, p. 273–313.

Mpodozis, C., Clavero, J, Quiroga, R., Droguett, B., and Arcos, R., 2018, Geología del área Cerro Cadillal-Cerro Jotabeche, Región de Atacama. Escala 1:100,000: Servicio Nacional de Geología y Minería, Carta Geológica de Chile, Serie Geología Básica 200, 94 p.

Munizaga, F., Maksaev, V., Fanning, C.M., Yaxley, G., and Tassinari, C.C.G., 2008, Late Paleozoic-Early Triassic magmatism on the western margin of Gondwana: Collahuasi area, Northern Chile: Gondwana Research, v. 13, p. 407–427.

Muntean, J.L., and Einaudi, M.T., 2001, Porphyry-epithermal transition: Maricunga belt, northern Chile: Economic Geology, v. 96, p. 743–772.

Murakami, H., Seo, J.H., and Heinrich, C.A., 2010, The relation between Cu/Au ratio and formation depth of porphyry-style Cu-Au ± Mo deposits: Mineralium Deposita, v. 45, p. 11–21.

Nasi, C., Mpodozis, C., Cornejo, P., Moscoso, R., and Maksaev, V., 1985, El Batolito Elqui-Limarí (Paleozoico superior-Triásico): Características petrográficas, geoquímicas y significado tectónico: Revista Geológica de Chile, no. 25–26, p. 77–111.

Palape, C., Coloma, F., Salazar, E., and Moisan, P., 2015, Nuevos antecedentes geocronológicos y estructurales de la Formación Las Placetas (Devónico-Carbonífero), Cordillera Principal, 29°S [ext. abs.]: Congreso Geológico Chileno, 14th, La Serena, 2015, Extended Abstracts, v. 1, p. 214–217.

Panteleyev, A., and Cravero, O., 2001, Faja del Potro and Cordón de la Brea ore deposits, La Rioja and San Juan: Radiometric dating, analytical results and sample documentation: Servicio Geológico Minero Argentino (SEGEMAR), Serie Contribuciones Técnicas, Recursos Minerales 11, 56 p.

Perelló, J., Urzúa, F., Cabello, J., and Ortiz, F., 1996, Clustered, gold-bearing Oligocene porphyry copper and associated epithermal mineralization at La Fortuna, Vallenar region, northern Chile: Society of Economic Geologists Special Publication 5, p. 81–90.

Perelló, J., Rojas, N., Devaux, C., Fava, L., Etchart, E., and Harman, P., 1998, Discovery of the Agua Rica porphyry Cu-Mo-Au deposit, Catamarca Province, northwestern Argentina. Part II: Geology, *in* Porter, T.M., ed., Porphyry and hydrothermal copper and gold deposits: A global perspective: Adelaide, Australian Mineral Foundation, p. 117–132.

Perelló, J., Mpodozis, C., and Urzúa, F., 2003, Late Oligocene-early Miocene porphyry Cu-Mo and Cu-Au mineralization, Pulido cluster, Atacama Region, northern Chile [abs.]: Congreso Geológico Chileno, 10th, Concepción, 2003, CD-ROM, 1 p.

Perelló, J., Sillitoe, R.H., Mpodozis, C., Brockway, H., and Posso, H., 2012, Geologic setting and evolution of the porphyry copper-molybdenum and copper-gold deposits at Los Pelambres, central Chile: Society of Economic Geologists Special Publication 16, p. 79–104.

Perelló, J., González, A., and Monroy, C., 2018, Geologic controls on hypogene mineralization at the Zaldívar porphyry copper-gold-molybdenum deposit, Escondida district, northern Chile: Society of Economic Geologists Special Publication 21, p. 271–292.

Perucca, L., and Angillieri, Y.E., 2008, A preliminary inventory of periglacial landforms in the Andes of La Rioja and San Juan, Argentina, at about 28°S: Quaternary International, v. 190, p. 171–179.

Proffett, J.M., 2003, Geology of the Bajo de la Alumbrera porphyry copper-gold deposit, Argentina: Economic Geology, v. 98, p. 1535–1574.

——2009, High Cu grades in porphyry Cu deposits and their relationship to emplacement depth of magmatic sources: Geology, v. 37, p. 675–678.

Razique, A., Tosdal, R., and Bouzari, F., 2016, Anatomical similarities and differences between spatially associated porphyry copper-gold deposits at the Reko Diq H14 and H15 Complex, Balochistan, Pakistan: Society of Economic Geologists Special Publication 19, p. 259–278.

Rode, M., and Carrizo, M., 2007, La faja de pórfidos del Salado, entre Valle Ancho y Vicuña, provincias de Catamarca, La Rioja y San Juan: Asociación Argentina de Geólogos Economistas, Publicación Especial 1, p. 31–50.

Rode, M., Guitart, A., Sanguinetti, M., and Richard, F., 2015, El depósito tipo pórfido Cu-Au de Los Helados, III Región, Atacama, Chile [ext. abs.]: Congreso Geológico Chileno, 14th, La Serena, 2015, Extended Abstracts, v. 2, p. 373–376.

Rossel, K., Aguilar, G., Salazar, E., Martinod, J., Carretier, S., Pinto, L., and Cabré, A., 2018, Chronology of Chilean Frontal Cordillera building from geochronological, stratigraphic and geomorphological data insights from Miocene intramontane-basin deposits: Basin Research, v. 30, p. 289–310.

Runyon, S.E., Seedorff, E., Barton, M.D., Steele-MacInnis, M., Lecumberri-Sanchez, P., and Mazdab, F.K., 2019, Coarse muscovite veins and alteration in porphyry systems: Ore Geology Reviews, v. 113, 103045, doi.org/10.1016/j.oregeorev.2019.103045.

Salazar, E., and Coloma, F., 2016, Geología del área Cerros de Cantarito-Laguna Chica, Región de Atacama. Escala 1:100,000: Servicio Nacional de Geología y Minería, Carta Geológica de Chile, Serie Geología Básica 181, 171 p.

Sato, A.M., Llambías, E.J., Basei, M.A.S., and Castro, C.E., 2015, Three stages in the Late Paleozoic to Triassic magmatism of southwestern Gondwana, and the relationships with the volcanogenic events in coeval basins: Journal of South American Earth Sciences, v. 63, p. 48–69.

Schirra, M., Laurent, O., Zwyer, T., Driesner, T., and Heinrich, C.A., 2022, Fluid evolution at the Batu Hijau porphyry Cu-Au deposit, Indonesia: Hypogene sulfide precipitation from a single-phase aqueous magmatic fluid during chlorite–white-mica alteration: Economic Geology, v. 117, p. 979–1012.

Setyandhaka, D., Arif, J., and Proffett, J., 2008, Characteristics of the roots of a classic copper-gold porphyry system—the Batu Hijau copper-gold porphyry deposit, Indonesia [ext. abs.]: Pacrim Congress 2008, Gold Coast, Queensland, 2008, Extended Abstracts: Melbourne, Australasian Institute of Mining and Metallurgy, p. 445–450.

Sillitoe, R.H., 1977, Permo-Carboniferous, Late Cretaceous and Miocene porphyry copper-type mineralization in the Argentinian Andes: Economic Geology, v. 72, p. 99–103.

——1979, Some thoughts on gold-rich porphyry copper deposits: Mineralium Deposita, v. 14, p. 161–174.

——1985, Ore-related breccias in volcanoplutonic arcs: Economic Geology, v. 80, p. 1467–1514.

——1993, Gold-rich porphyry copper deposits: Geological model and exploration implications: Geological Association of Canada Special Paper 40, p. 465–478.

——1994, Erosion and collapse of volcanoes: Causes of telescoping in intrusion-centered ore deposits: Geology, v. 22, p. 945–948.
——1995, Exploration of porphyry copper lithocaps: Pacific Rim Congress, Auckland, 1995, Proceedings: Melbourne, Australasian Institute of Mining and Metallurgy, p. 527–532.
——1998, Major regional factors favouring large size, high hypogene grade, elevated gold content and supergene oxidation and enrichment of porphyry copper deposits, *in* Porter, T.M., ed., Porphyry and hydrothermal copper and gold deposits: A global perspective: Adelaide, Australian Mineral Foundation, p. 21–34.
——2000, Gold-rich porphyry deposits: Descriptive and genetic models and their role in exploration and discovery: Reviews in Economic Geology, v. 13, p. 315–345.
——2005, Supergene oxidized and enriched porphyry copper and related deposits: Economic Geology 100th Anniversary Volume, p. 723–768.
——2009, Supergene silver enrichment reassessed: Society of Economic Geologists Special Publication 14, p. 15–32.
——2010, Porphyry copper systems: Economic Geology, v. 105, p. 3–41.
Sillitoe, R.H., and Perelló, J., 2005, Andean copper province: Tectonomagmatic settings, deposit types, metallogeny, exploration, and discovery: Economic Geology 100th Anniversary Volume, p. 845–890.
Sillitoe, R.H., McKee, E.H., and Vila, T., 1991, Reconnaissance K-Ar geochronology of the Maricunga gold-silver belt, northern Chile: Economic Geology, v. 86, p. 1261–1270.
Sillitoe, R.H., Tolman, J., and Van Kerkvoort, G., 2013, Geology of the Caspiche porphyry gold-copper deposit, Maricunga belt, northern Chile: Economic Geology, v. 108, p. 585–604.
Sillitoe, R.H., Burgoa, C., and Hopper, D.R., 2016, Porphyry copper discovery beneath the Valeriano lithocap, Chile: Society of Economic Geologists, SEG Newsletter 106, p. 1, 15–20.
Sillitoe, R.H., Devine, F.A.M., Sanguinetti, M.I., and Friedman, R.M., 2019, Geology of the Josemaría porphyry copper-gold deposit, Argentina: Formation, exhumation, and burial in two million years: Economic Geology, v. 114, p. 407–425.
Steven, T.A., and Ratté, J.C., 1960, Geology and ore deposits of the Summitville district, San Juan Mountains, Colorado: U.S. Geological Survey Professional Paper 343, 70 p.
Torres, M.G., Rubinstein, N., Poole, G., and Hagemann, S., 2020, Adakitic signal linked to Gondwanan porphyry type deposits from the Andean Frontal Cordillera of Argentina: Geochemistry, v. 80, 125634. doi.org/10.1016/j.chemer.2020.125634.
Vila, T., and Sillitoe, R.H., 1991, Gold-rich porphyry systems in the Maricunga belt, northern Chile: Economic Geology, v. 86, p. 1238–1260.
Winocur, D.A., Litvak, V.D., and Ramos, V.A., 2015, Magmatic and tectonic evolution of the Oligocene Valle del Cura basin, main Andes of Argentina and Chile: Evidence for generalized extension: Geological Society, London, Special Publications, v. 399, p. 109–130.
Yoshie, T. Otsubo, T., Oku, N., and Ueda, Y., 2015, Exploration and resource estimation of the Caserones porphyry Cu-Mo deposit in III Region, Chile: Shigen-Chishitsu, v. 65, p. 53–79 (in Japanese with English abs.).

José (Pepe) Perelló gained a B.Sc. degree from Universidad de Chile, Santiago, Chile, and an M.Sc. degree from Queen´s University, Kingston, Ontario, Canada. He worked for 18 years with BHP and 22 years with Antofagasta Minerals. With both companies, he was involved in all exploration stages of numerous base metal deposits, mainly porphyry and sediment-hosted copper, in more than 50 countries worldwide. Pepe took retirement in 2021 and is currently a part-time independent consultant in economic geology and exploration, based in Santiago, Chile.